5-2018

Design of a Multidirectional Wear Testing Device for Simulating Wear of Biocompatible Materials Used in Joint Implants

Carlos A. Rodriguez Betancourth
The University of Texas Rio Grande Valley

DESIGN OF A MULTIDIRECTIONAL WEAR TESTING DEVICE

FOR SIMULATING WEAR OF BIOCOMPATIBLE MATERIALS

USED IN JOINT IMPLANTS

A Thesis

by

CARLOS A. RODRIGUEZ BETANCOURTH

Submitted to the Graduate College of
The University of Texas Rio Grande Valley
In partial fulfillment of the requirements for the degree of

MASTER OF SCIENCE IN ENGINEERING

May 2018

Major Subject: Electrical Engineering

DESIGN OF A MULTIDIRECTIONAL WEAR TESTING DEVICE

FOR SIMULATING WEAR OF BIOCOMPATIBLE MATERIALS

USED IN JOINT IMPLANTS

A Thesis
by
CARLOS A. RODRIGUEZ BETANCOURTH

COMMITTEE MEMBERS

Dr. Javier Ortega
Co-Chair of Committee

Dr. Hasina Huq
Co-Chair of Committee

Dr. Jaime Ramos
Committee Member

May 2018

ABSTRACT

Rodriguez Betancourth, Carlos A., Design of a Multidirectional Wear Testing Device For Simulating Wear of Biocompatible Materials Used in Joint Implants. Master of Science in Engineering (MSE), May, 2018, 80 pp, 53 figures, references, 28 titles.

In the present work, a novel multidirectional pin-on-disc wear testing device designated CNC-POD (computer-numerical-control pin-on-disc) capable of replicating the cross-shear motions experienced by a prosthesis in vivo was designed and developed in the UTRGV in order to evaluate the wear resistance of new biomaterials. The CNC-POD consists of six temperature-controlled pin-on-disc stations mounted on a two-axis CNC table (X-Y). Each pin-on-disc station is load-programmable up to 500 Newtons (115 pounds). The CNC table allows the machine to reproduce a wide range of 2D patterns in millimeter scale on the six stations under a specific load. Friction force is measured during testing using force sensors and coefficient of friction can be calculated. Motions and loads are fully programmable through LabVIEW.

DEDICATION

I want to thank to my parents and brother for always giving me their unconditional support, to my wife for believe in me and supporting me since I was studying my bachelor's degree. Thanks to all of you.

AKNOWLEDGEMENTS

I want to extend my gratitude to Dr. Javier Ortega for proposing me to work beside him in this project, to Dr. Jaime Ramos for encouraging me to further my education here at UTRGV, to Dr. Hasina Huq for welcoming me in the UTRGV Electrical Engineering Graduate program, and to Mr. Hector Arteaga for his assistance and advisement in the manufacturing process of this project.

TABLE OF CONTENTS

LIST OF TABLES

LIST OF FIGURES

CHAPTER I

INTRODUCTION

1.1 Statement of the Problem

One of the main causes of joint prostheses failure is the premature wear of its components. Ultra-high molecular weight polyethylene (UHMWPE) is worldwide used as a bearing material in orthopedic implants. Multi-directional motion or "cross-shear" motion has been identified as one of the most significant factors affecting the wear rate of UHMWPE in total hip joint replacement prostheses. It has been found that the trajectory of motion at the point of contact between a femoral head and an acetabular cup takes a general quasi-elliptical or rectangular shape during a gait cycle.

1.2 Statement of Purpose

The main objective of this project is the design and development of a new wear testing device, with unidirectional and bidirectional motion, that reproduce experiments and test carried out on different existing devices and wear simulators to compare the results obtained by implementing the same parameters and materials during the test. LabVIEW, as a virtual instrument to control and monitor the device, supports the design.

There are six chapters in this thesis, where it can be seen the work developed through this research, each chapter is going to present a new step in the way to get the desired results.

In chapter two, a general background of wear testing devices that simulate motion of hip joint is given, different experiments that have been developed on them, as well as the parameters that have been implemented on simulations and the obtained results. In this chapter it can be seen what a hip joint implant or total hip replacement represents, the new bio compatible materials that are involved on this implants, and different types of tribometers.

In chapter three, the composition of the device is established, based on the parameters that needs to be evaluated through the experiments. It defines the components, either electrical or mechanical, their function on the device and the subsystems that they conform within the device. A first prototype is presented, in order to verify the whole operation of the components like the linear actuator, the linear motion mechanism and the load cells that allows to measure the coefficient of friction, on a single station device. After the obtained results on the first prototype, the main devices is developed following the design established on chapter three.

In chapter four, experimental procedures are carried out, in order to verify the operation of the developed device; these procedures are based on the regulation ASTM G133.

In chapter five the results of all the experimentation, starting from the first prototype, to the six stations device, are presented, showing the functionality of both devices and the differences in the operation between them.

In chapter six, a conclusion is reached, regarding all the work presented through this document, a comparison between desired results and obtained results and what produces it, is developed and the possible future work is described.

CHAPTER II

LITERATURE REVIEW

2.1 The hip joint

The hip joint, scientifically referred to as the acetabulofemoral joint (art. coxae), is the joint between the femur and acetabulum of the pelvis and its primary function is to support the weight of the body in both static (e.g. standing) and dynamic (e.g. walking or running) postures. It is formed by the iliac bone or innominate bone as well as by a capsule and the ligaments that protect it []. The hip joints are the most important part in retaining balance. The pelvic inclination angle, which is the single most important element of human body.

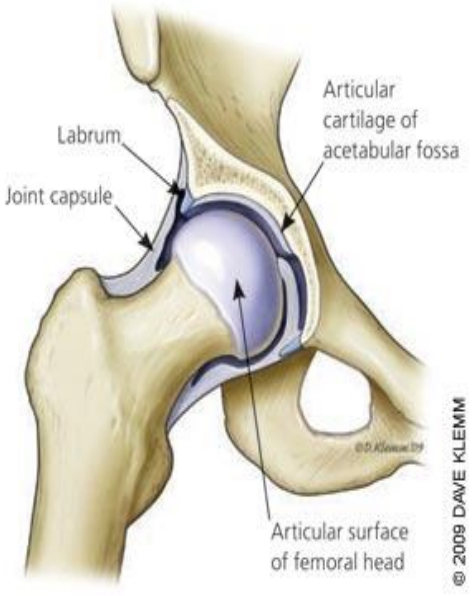

Figure 2.1. - Human Hip Joint.

2.1.1 Hip fracture

A hip fracture is a break in the upper quarter of the femur (thigh) bone. The extend of the break depends on the forces that are involved. A hip fracture almost always requires surgical repair or replacement.

Figure 2.2. - Hip Fracture.

2.2 Hip joint implant

The hip joint implant is the prosthetic system that has been widely studied for being the first articulation which replacement was done in first place in a massive way and with a relative success.

Hip replacement surgery, known in medical terms as arthroplasty of hip surgery, consists of orthopedic surgery that seeks to replace totally or partially the articulation of the hip with artificial implants (prosthesis), aiming at the pain relief and recovery of mobility. The basic

components of a hip prostheses are: the femoral stem, artificial head or ball attached to this stem and the artificial acetabulum that attaches to the pelvis.

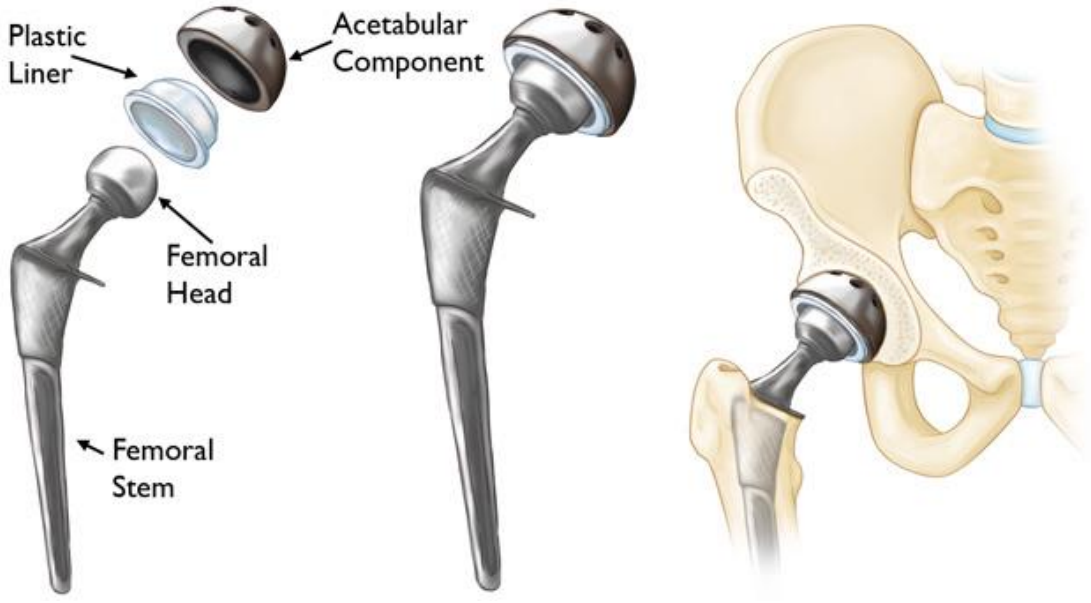

Figure 2.3. - Hip Joint Implant.

The hip prostheses can be classified by:

- The way that they are attached on to the patient's bone
- According to the material of which the head of the femur and the acetabular cup are made.

According to the material of which the head of the femur and the acetabular cup are made, the total hip replacement can be classified by:

- Metal – metal, if both of the parts are metallic;
- Metal – polyethylene, if the acetabulum is made of polyethylene and the head is metallic;

- Polyethylene – ceramic, if the acetabulum is made of polyethylene and the head is made of ceramic.
- Ceramic – ceramic, if both of them are made of ceramic.

2.3 Materials used in total hip replacements

The human body is a living system that works in a very complex and perfect way, currently science and technology allow, that an artificially manufactured organism can replace when any of the organisms that compose it fails or is damaged. However, when making these artificial organisms, it is necessary to consider certain restrictions, starting with the materials that are used to be implanted in the human body, since these have to be biocompatible, which means that they have a probability minimum of being rejected by the body. For example, in the case of metal alloys, it is necessary to consider that the body fluids are highly corrosive, so the material used, must be resistant to this. The **Figure 2.4** shows the most common biocompatible materials and their classification.

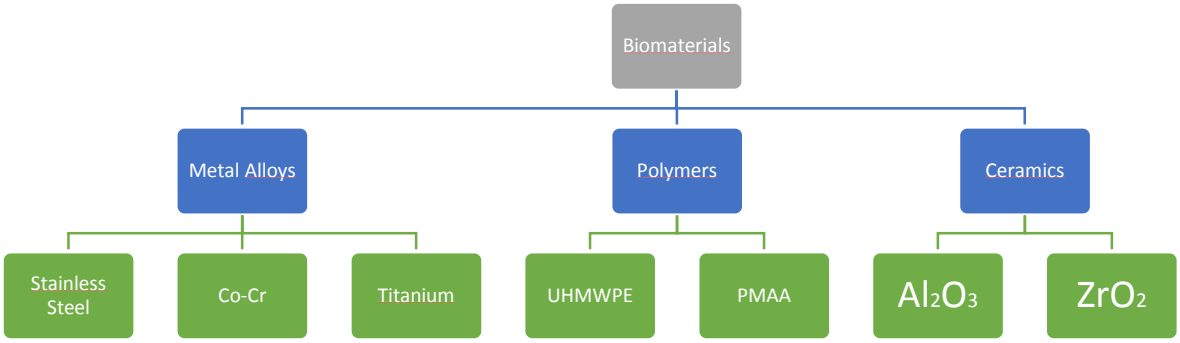

Figure 2.4. – Materials Used In Surgical Implants.

On the other hand, since the implant is designed for a joint, the mechanical properties of each selected material must be considered, that the components are light and that the properties of the materials used are stable over time. Ideally, an implanted hip prosthesis should function satisfactorily throughout the patient's life in a way that is not necessary replacement, but in the current designs the life of the prosthesis varies between 10 and 15 years, certainly longer time is required.

The hip joint is a mechanism composed of two parts that are in constant contact, motion, friction and wear are results of these constant interactions, and as is mentioned in the introduction, premature wear in the components, can cause the failure of the prostheses. All of these mentioned factors are present when selecting suitable materials for making a hip joint implant. **Table 2.1** below shows the biocompatible materials that are suitable for this type of implant, as well as their mechanical properties.

The acetabular part of the hip implants is currently fabricated with alloys of Co – Cr or Ti, but since the total arthroplasty was implemented, the most common material used is the ultra-high molecular weight polyethylene (UHMWPE).

Table 2.1 Mechanical Properties Of Biocompatible Alloys.

Alloy	Yield Strenght (MPa)	Tensile Strenght (MPa)	Elongation E (%)	Elastic Module (GPa)
Stainless Steel 316L	170	485	40	193
Stainless Steel 316L (Cold worked)	689	862	12	200
Co – Cr (F75)	558	1013	30	248
Co – Cr (Worked + annealed)	379	897	-	242
Titanium Grade 4	485	550	15	110
Ti – 6Al – 4V (Annealed)	1070	1100	10	114
UHMWPE	40	38	200	0.82
PMAA	0	70	2.5	4.629
Alumina (Al_2O_3)	-	69	-	300
Zirconia (ZrO_2)	230	330	32	115

Table 2.2 Typical Coefficients Of Friction For Clean Materials In Dry Contact.

Material combination	Coefficient of friction
Steel on Steel	0.6 – 0.8
Polyethylene on Steel	0.3
Polyethylene on Polyethylene	0.2 – 0.4
Ceramic on Ceramic	0.04 – 0.2
Ceramic on Steel	0.04 – 0.2

The third law of friction is generally attributed to Coulomb in 1785. The kinetic coefficient of friction is generally less than or equal to the static coefficient of friction. Typical static coefficients of friction for clean materials in dry contact in the presence of air are given in **Table 2.2**. It should be pointed out that the coefficient of friction depends significantly on the nature of the bearing surfaces, particularly in the presence of biological lubricants. **Table 2.3** summarizes the typical friction factors on different hip joints in the presence of bovine serum.

Table 2.3 Typical Coefficients Of Friction For Bearings For Artificial Human Joint.

Material combination	Friction
UHMWPE on metal	0.06 – 0.08
UHMWPE on ceramic	0.06 – 0.08
Metal on metal	0.22 – 0.27
Ceramic on Ceramic	0.002 – 0.07
Ceramic on metal	0.002 – 0.07

2.4 Tribometers

The word tribology derives from the Greek root τριβ- of the verb τρίβω, tribo, "I rub" in classic Greek; and the suffix –loggy from –λογία, -logia "study of", so the literal translation will be "Rubbing Science". Tribology is the science and technology that studies the lubrication, friction and wear of moving or stationary parts. Lubrication, friction and wear have a fundamental function in the life of the machine element.

A tribologic machine or tribometer, is a testing and simulation device of friction, wear and lubrication which are the object of study of tribology [].Usually tribometers are very specific in their functions since they simulate certain movements to which the material to be tested would be subjected, in order to be able to study in the aforementioned variables. According to the shape of contact surface between test materials, also called "tribologic pair", and the motion that the device generates, tribometers can be classified as: Pin on disk, Reciprocating, Multi – axis and Simulators just to mention some of them.

2.4.1 Pin on disk tribometer

A Pin on disk tribometer consist on a stationary "pin" under applied load in contact with a rotating disk. The pin can have any shape to simulate a specific contact, but spherical tips are often used to simplify the contact geometry. Coefficient of friction is determined by the ratio of the frictional force to the loading force on the pin.

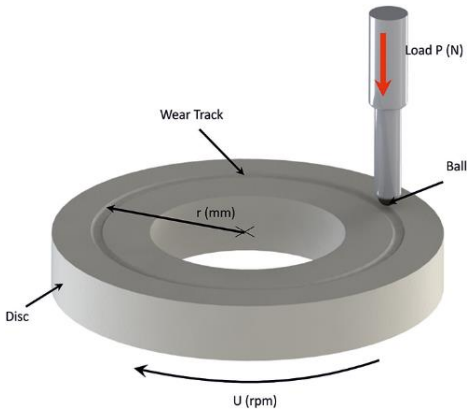

Figure 2.5. – General Schematic Of A Pin On Disk.

2.4.2 Reciprocating tribometer

Within the different types of movement that describe the mechanisms, there is one that by its nature makes it the most complex to understand. The reciprocating movement is present in most mechanical systems. A reciprocating machine, is a tribometer where a pin, under applied load, slides on a linear and reciprocating way on the surface of a flat specimen. The load is applied vertically to the plate through the pin.

Figure 2.6. – Reciprocating Tribometer Model T-17 From The Institute For Sustainable Technologies.

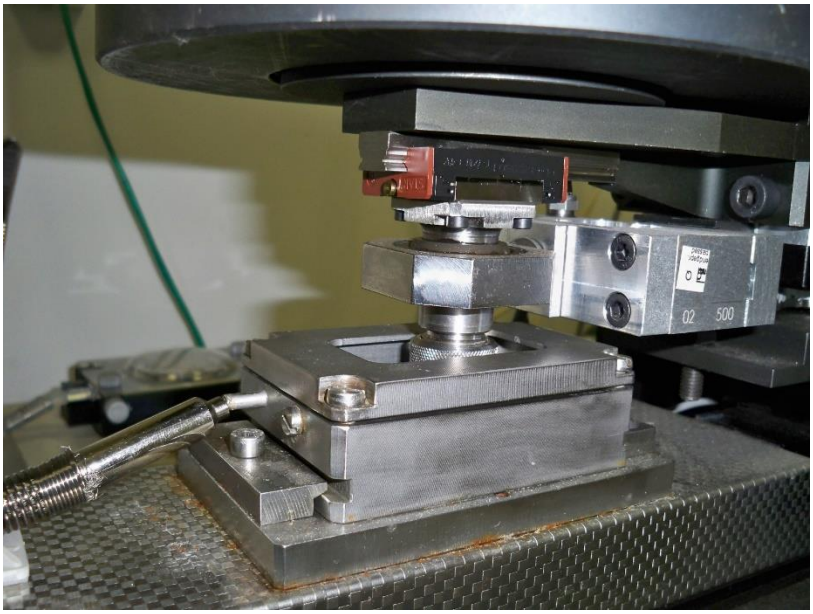

Figure 2.7. - Extended View To The Chamber Of The Reciprocating Tribometer T-17.

2.4.3 Multi-axis tribometer

A multi – axis tribometer, is a wear testing device that can be set up to work as a pin on disk, or reciprocating plate configurations depending on the experiment to be performed. The CNC – POD is classified in this category since its characteristics allows it to be set up as any of the mentioned before tribometers. One example of this type of tribometers is the OrthoPOD developed by the company AMITI, this machine is capable of replicating the complex motions essential for accurately simulating the in vivo wear of polyethylene joint implants. **Figure 2.8** shows the OrthoPOD device.

Figure 2.8. – Orthopod Tribometer Developed By AMITI.

2.4.4 Simulators

A simulation process is the collection of available information of a real system and a test system, in this case, the real system is represented by the human hip joint and the test system is represented by a hip simulator. A successful simulation requires similitude between the function of the real system and the operation of the test system. The hip simulators, are wear testing devices designed for study the tribological performance of biocompatible materials implemented on total hip joint implants.

According to the movement that they do, hip simulators cab be classified as:

- Uniaxial, reproducing just FE.
- Biaxial, reproducing FE and AA.
- Triaxial, reproducing FE, AA and IER.

The **Figure 2.9** shows a hip simulator with biaxial reciprocating motion, where it can appreciate the acetabular cup, the femoral head, the antirotation arm, the rotating base and the lubricant container.

Figure 2.9. – Hip Joint Simulator With Biaxial Reciprocating Motion (BRM), HUT – 3.

The kinematics of the human hip joint is reproduced with greater precision in triaxial simulators with respect to uniaxial hip simulators (pure flexion-extension).

2.5 Wear testing

To carry out a wear test, there is a regulation that depends on the type of study that is intended to perform. The American Society for Testing and Materials (ASTM) stablishes the Standard Test Methods for testing procedures with the different devices.

2.5.1 ASTM F732

The ASTM F732 is the Standard Test Method for Wear Testing of Polymeric Materials used in Total Joint Prostheses. This test method describes a laboratory method for evaluating the wear properties of combinations of materials that are being considered for use as bearing surfaces of human total joint prostheses.

2.5.1.1 Apparatus and Materials. ASTM F732 describes that the standard polymer specimen is a flat-ended circular cylinder 13 mm (0.50 in) long and 9 mm (0.354 in) diameter, providing a cross-sectional area of 63.6 mm^2 (0.0986 in^2). In the wear machine, the polymer specimen is loaded end-wise against the counterface in flat-on-flat configuration.

In the case of a multiple specimen machine, the specimens must be contained in individual isolated chambers to prevent contamination. Each chamber must be made entirely of corrosion- resistant materials and must be easily removable from the machine for thorough cleaning between tests.

2.5.1.2 Load. The test load of 225 N (50.6 lbf) should be applied along the longitudinal axis of the polymer specimen. The loading apparatus must be free to follow the specimen as wear occurs, such that the applied load is constant to within +/- 3% for the duration of the test.

2.5.1.3 Motion. The orientation between sliding direction and the lay of the surface roughness in each test should be noted.

2.5.1.4 Sliding Speed. Specimens should be run through 25 mm stroke at a rate of 1 cycle/s (1 Hz), producing an average sliding speed of 50 mm/s.

2.5.1.5 Cycle counter. The machine should include a cycle counter to record the total number of wear cycles.

2.5.1.6 Friction. It is recommended that the machine include stain gage instrumentation or other transducers capable of providing a continuous read out of the tangential (friction) force transmitted across the specimen interface during the test.

2.5.1.7 Lubricant. The F732 method specifies that the specimen must be lubricated with bovine blood serum unless an alternative medium can be justified, since different in composition, dilution with deionized water of up to 75% may be appropriate; serum must be filtered to remove hard, abrasive, particulate contaminants that might be otherwise affect the wear properties of the specimen begin tested

2.5.2 ASTM G133-95

The ASTM G133-95 is the Standard Test Method for Linearly Reciprocating Ball-on-Flat Sliding Wear. This test method describes laboratory procedures for determining the sliding wear of ceramics, metals and other candidate wear-resistant materials using a linear, reciprocating ball on flat plane geometry. The method encompasses both unlubricated and lubricated testing procedures.

2.5.2.1 Apparatus and Materials. ASTM G133 describes that pin tip is a ball specimen with a diameter of 3/8”. In the wear machine, the ball specimen may be a fixed bearing ball or any spherically tipped specimen as long as the sliding contact is equivalent to a ball on flat plane.

In the case of a multiple specimen machine, the specimens must be contained in individual isolated chambers to prevent contamination. Each chamber must be made entirely of

corrosion- resistant materials and must be easily removable from the machine for thorough cleaning between tests.

2.5.2.2 Load. The test load of 225 N (50.6 lbf) should be applied along the longitudinal axis of the ball specimen. The loading apparatus must be free to follow the specimen as wear occurs, such that the applied load is constant to within +/- 3% for the duration of the test.

2.5.2.3 Motion. The orientation between sliding direction and the lay of the surface roughness in each test should be noted.

2.5.2.4 Sliding Speed. Specimens should be run through 25 mm stroke at a rate of 5 cycle/s (5 Hz), producing an average sliding speed of 250 mm/s.

2.5.2.5 Cycle counter. The machine should include a cycle counter to record the total number of wear cycles.

2.5.2.6 Friction. It is recommended that the machine include stain gage instrumentation or other transducers capable of providing a continuous read out of the tangential (friction) force transmitted across the specimen interface during the test.

2.5.2.7 Lubricant. The G133 method specifies that the specimen can be unlubricated, lubricated or in a full immersion of lubricant. It does not specify a lubricant to use.

2.5.3 ASTM G99

The ASTM G133-95 is the Standard Test Method for Wear Testing with a Pin-on-Disk Apparatus. This test method describes a laboratory procedure for determining the wear of

materials during sliding using a pin-on-disk apparatus, Material are tested in pairs under nominally non-abrasive conditions.

2.5.3.1 Apparatus and Materials. One type of typical system consist of a driven spindle and chuck for holding the revolving disk, a lever-arm device to hold the pin, and attachments to allow the pin specimen to be forced against the revolving disk specimen with controlled load. Another type of system loads a pin revolving about the disk center against a stationary disk. In any case the wear track on the disk is a circle.

2.5.3.2 Rotating Speed. Speeds are typically in the range 0.3 to 3 rad/s (60 to 600 r/min).

2.5.3.3 Revolution counter. The machine should include a revolution counter to record the total number of disk revolutions, and preferable have the ability to shut off the machine after a pre-selected number of revolutions.

2.5.3.6 Friction. The system may have a friction force measuring system that allows the coefficient of friction to be determined.

2.5.4 Summary of wear test performed on different devices

Throughout the years, various specialists in the area of tribology have developed wear tests, implementing different devices, both commercial and developed by themselves. Despite having the same purpose of studying the wear on hip implants, each one employed different types of tribometers as shown in **Table 2.2**, that it is a summary of the most outstanding wear tests performed on tribometers.

Table 2.4. –Summary Of Wear Tests Performed On Different Devices

Authors	Bragdon, C.	Escudeiro, A. Wimmer, M.	Turell, M. Friedlaender, G. Wang, A. Thornhill, T. Bellare, A.	Turell, M.	Korduba, L.A. Wang, A.	**ASTM F732**	**ASTM G133**	**ASTM G99**
Disk (Alloy)		Ti grade 5 (Ti_6Al_4V)	CoCr	CoCr	CoCr			**Steel/ Alumina**
Pin (Material)	Nonirradited PE	UHMWPE (GUR 1050)	UHMWPE (GUR 1050)	UHMWPE (GUR 1050)	UHMWPE (GUR 1050)			**Steel/ Alumina**
Disk diameter (mm)	30	40	25	25	25.4			**40**
Disk height (mm)			3	3	6.4			
Pin diameter (mm)	9	9.525	9	9	9.525	**9**		**10**
Pin length (mm)	20	19.1	20	20	25.4	**13**		**10**
Load (N)	310	106.32	192	192	75	**225**	**25/200**	
Load (Kg)	31.685	10.84	19.57	19.57	7.64	**22.93**	**2.54/ 20.39**	
Contact pressure (MPa)	4.885	1.5	3	3.018	1.05	**3.54**		
Number of cycles (million)	2	2	1	1	1	**2**	**0.004/ 0.016**	
Wear Track (mm)	5 x 10	15 x 15					**25**	
Frequency (Hz)	2, 1	1	1	1	1	**1**	**5/10**	

CHAPTER III

METHODOLOGY AND DESIGN

3.1 Introduction

As mentioned in the introduction of this document, the main objective of the project is the creation of a testing device capable to evaluate the wear and friction properties of different material combinations with bidirectional sliding motion and subjected to a constant load in a lubricated environment. After analyzing and studying different devices found on the literature, it was proposed to develop a design including several systems operating in a joint way that would allow to perform a bidirectional motion while applying a specific load, using a pin-on-disc configuration.

3.2 Design of the CNC – POD

Considering the information presented in the previous chapters, it was determined to design and develop a bidirectional device that allows the study of the tribological properties of biocompatible materials intended for hip and knee implants, and also it can be used as a universal testing device to perform tribological tests following the specifications included in different standards such as ASTM F732, ASTM G133, and ASTM G99. The proposed device was denominated CNC-POD (Computer-Numerical-Control Pin-On-Disc). The design of the CNC-POD is based mainly on specific features that meet the requirements established by the standards mentioned before. Those features are described in full detail in the following lines.

3.2.1 Six testing stations

The idea of having six stations on the same device, allow us to perform a test on six specimens simultaneously, reducing time and results on each station can be compared in vivo or at the end of the test.

Following the specifications described on the ASTM F732 standard about the specimen chambers, each chamber is isolated from the others and is composed by three parts: the specimen holder, the base of the specimen holder, and the container. The three of them are designed to be manufactured on stainless steel. **Figure 3.1** shows the composition of a specimen chamber.

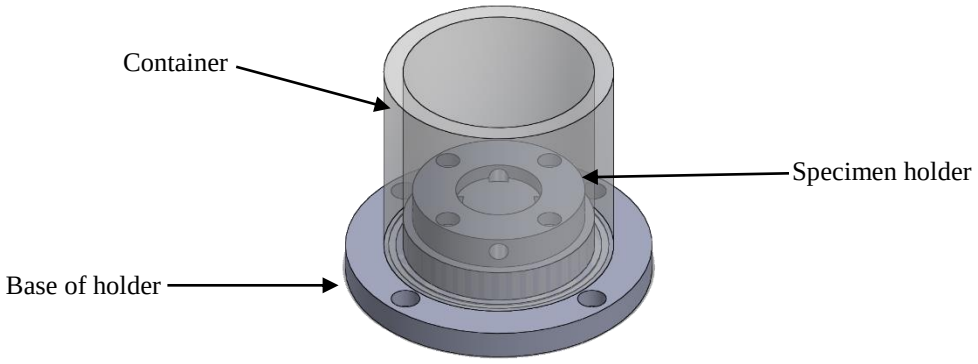

Figure 3.1. – Specimen Chamber.

The six specimen chambers are installed on another stainless-steel container as shown in **Figure 3.2.** The purpose of this container is to be filled with a fluid at a specific temperature. The fluid circulates around the chambers maintaining the same temperature on them.

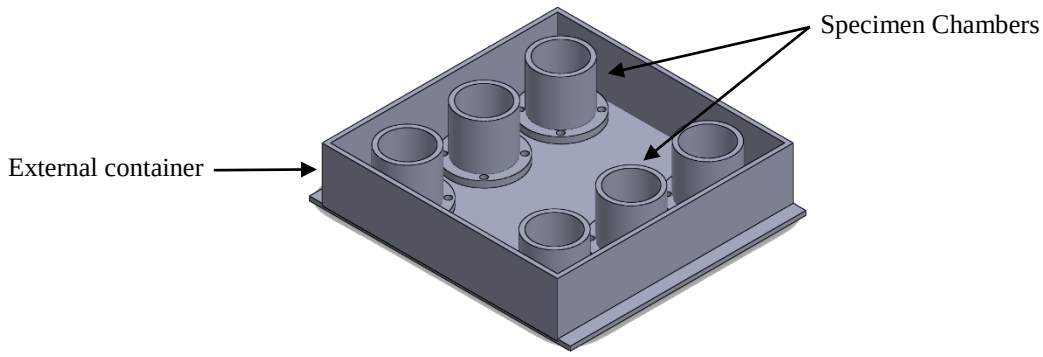

Figure 3.2. – Chambers Container.

3.2.2 Two-dimensional patterns

As mentioned in the introduction of this document, cross-shear motion has been identified as one of the most significant factors of wear in UHMWPE. It is desired that the present wear testing device will be able to perform motion in two directions, and it must have the capacity to generate a wide range of patterns that allow the simulation of motion generated in those parts of the human body where implants are located; this in order to have more accurate results. Also, this system must have the facility to carry out the motion, and to do it at an adequate speed, even when it receives a specific load during its operation cycles. For all the mentioned above, it was decided to use a linear mechanism of two axes, also known as X-Y table, which consists of the conjunction of two axes mechanisms that operate linearly, one perpendicular to the other.

3.2.2.1 Motion system. The motion system consists in a X-Y table, which is a mechanism composed by two perpendicular linear axes (X and Y axis) which operate by software allowing the reproduction of bidirectional patterns. Each axis of the mechanism has a stepper motor connected to an endless screw where the last one converts the rotation on linear motion. The

endless screw drives the motion while the rest of the table is supported by four linear bearings that slides on two rails in each axis. This table was designed to be fabricated in Aluminum alloy 6061-T6 due to the resistance of the material and its light weight. The structure can support a load of 3.1 KN the endless screw has a resolution of 5 mm per revolution while the stepper motor resolution is up to 0.072°, which means that the minimum displacement is about 0.001 mm per step. Dimensions of the table are established so that each specimen chamber rests on the rails of the axis. **Figure 3.3** shows the final design of the motion system.

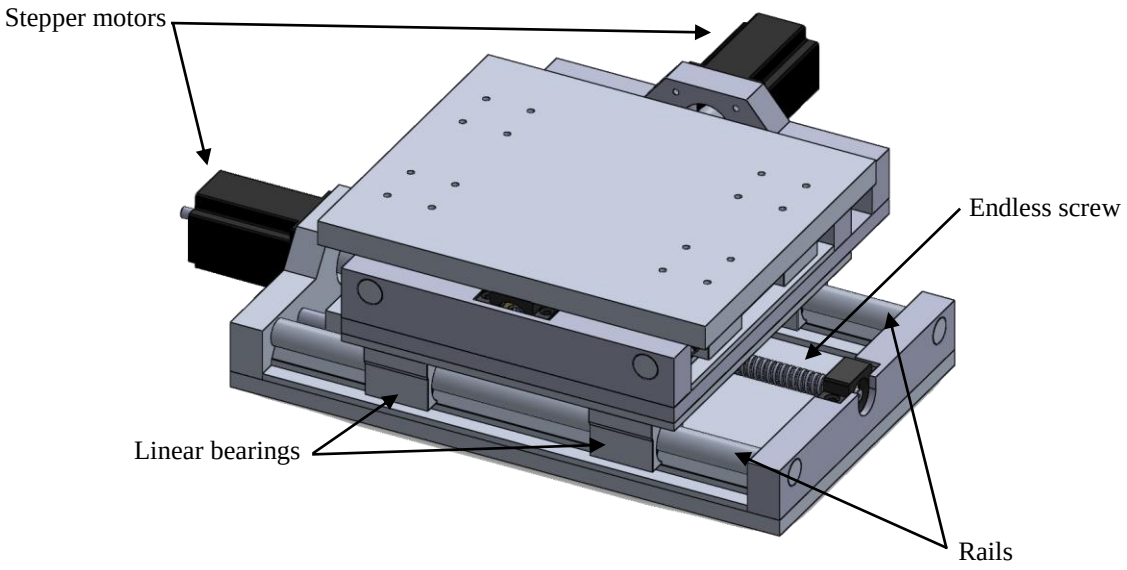

Figure 3.3. – X-Y Table Designed For Motion System.

The selected stepper motor was a NEMA 24 Stepper motor model 24HS39-3008D, it is classified as one of the strongest NEMA 24 motors, with a steep angle of 1.8 degrees and size 60 x 60 x 100 mm, which have three connection options: Unipolar or Bipolar (serial) or Bipolar (parallel). Its holding torque reach 2.8 N-m with unipolar connection and 4.0 Nm with bipolar

connection. The 24HS39-3008D is presented on **Figure 3.4**, and its technical specifications are presented on **Table 3.1**.

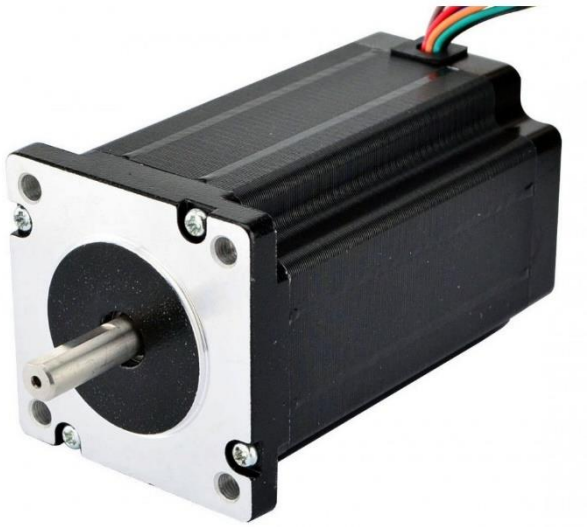

Figure 3.4. – NEMA 24 Stepper Motor 24HS39-3008D.

Table 3.1. - Stepper Motor Model 24HS39 – 3008D Properties.

Electrical Specification	
Bipolar/Unipolar	Bipolar
Step Angle (°)	1.8
Holding Torque (Nm)	4
Holding Torque (oz.in)	566
Rated current (A)	4.24
Phase resistance (Ω)	0.7
Inductance (mH)	3

3.2.3 Load application

During a test, a specific load has to be applied to the specimen in a constant way, while the specimen is displaced by the X-Y table reproducing the desired pattern. Load can be static, where the same weight is applied constantly during the test, or dynamic, where the load can variate, depending on a specific load cycle. In order to fill those requirements, a system with linear actuators was designed.

3.2.3.1 Load system. In this design, load is applied by six electric linear actuators, one by each station, and each one has the capacity to apply up to 500 Newtons of load. The load system has an individual control for each linear actuator which means that can be set up to apply different loads on each specimen if it is required. A linear actuator model 6-50 (**Figure 3.5**) was selected based on its specifications, which are listed on **Table 3.2.**

Figure 3.5. – Linear Actuator Model 6-50, 6” 500 N.

Table 3.2. - Electrical And Mechanical Properties Of Linear Actuator Model 6 – 50.

Supply Voltage (V)	6 – 12
Dynamic thrust (lbs)	115
Current Drain @ max load (A)	3.8
Feedback style	10KΩ Potentiometer
Potentiometer linearity (%)	0.25
Feedback density (Ω/in)	1.66 K
Gear ratio	20:1
Duty Cycle (%)	25

In the designed load system, each linear actuator is mounted on an adapter that connects the mounting bracket of the actuator to a linear bearing, this adapter holds a feedback load cell with a maximum capacity of 40 kg. The body of the linear actuator is held by a U-bolt which is directly connected to another linear bearing; this linear bearing, and the one mentioned before slides on a 12 mm rail which is parallel to the linear actuator, this configuration serves as a guide in order to prevent undesired motion at the time to apply the load. The stoke of each linear actuator goes through a 20 mm linear bearing that prevent it to move in another way but at the same time, supports a load cell that measure the force generated in the stroke by friction. A 3D model design of the conjunction of this actuator is presented on **Figure 3.6.**

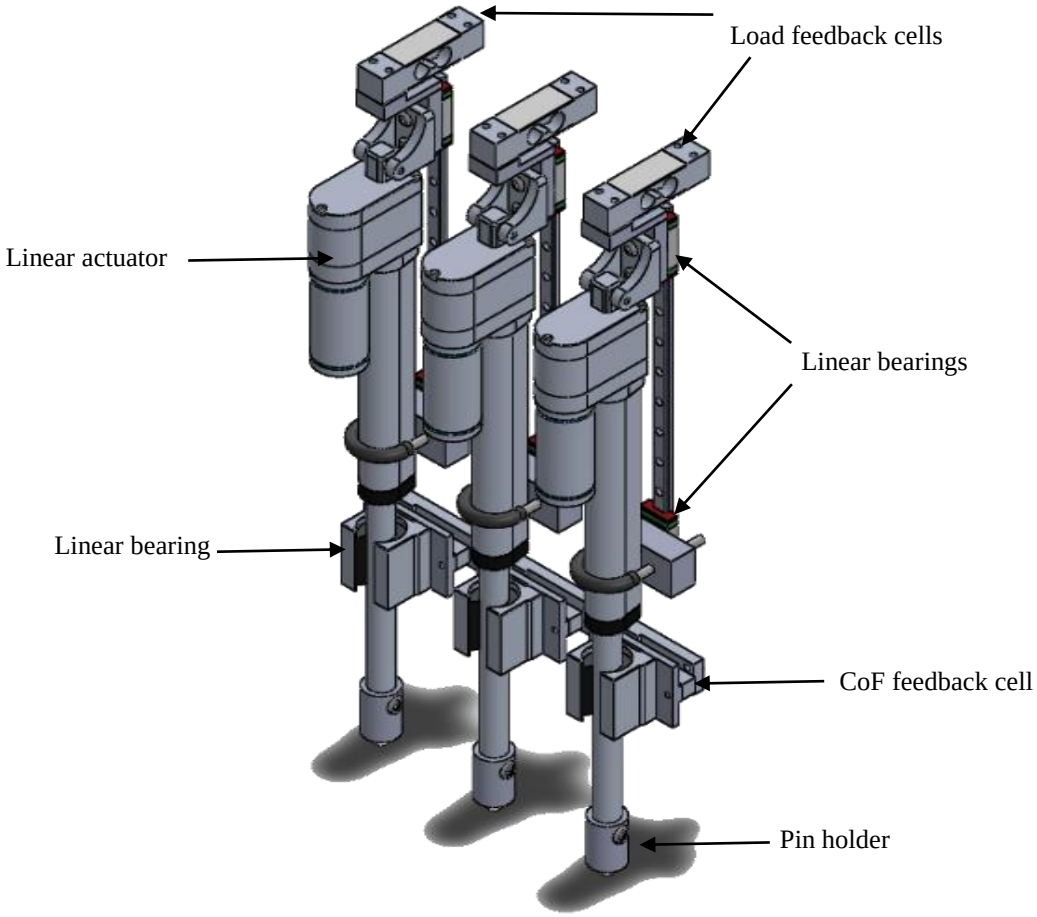

Figure 3.6. – Load Application System.

3.2.4 In vivo Coefficient of Friction determination

One of the recommendations on the ASTM standards (F732, G99 and G133) is that the wear testing device integrates the possibility to measure the friction generated between the pin and the specimen during a test. For this reason, it was decided to include a transducer capable to measure the force applied on it and reflect it on an electrical signal. As described on section 3.2.3.1, a load cell is installed in the stroke of each linear actuator to measure the force generated on it.

3.2.4.1 Load cell. A load cell is a transducer that is used to create an electrical signal whose magnitude is directly proportional to the measured force. The various load cell types include hydraulic, pneumatic, and strain gauge, being the last one chosen for this design.

A strain gauge load cell, consist in four strain gauges in a Wheatstone bridge configuration, the electrical signal output is in the order of millivolts and an instrumentation amplifier is needed to condition the output signal. The gauges themselves are bonded onto a beam or structural member that deforms when weight is applied. In most cases, four strain gauges are used to obtain maximum sensitivity and temperature compensation. Two of the gauges are usually in tension can be represented as T1 and T2, and two in compression can be represented as C1 and C2, and are wired with compensation adjustments. The strain gauge load cell is fundamentally a spring optimized for strain measurement. Gauges are mounted in areas that exhibit strain in compression or tension. When weight is applied to the load cell, gauges C1 and C2 compress decreasing their resistances. Simultaneously, gauges T1 and T2 are stretched increasing their resistances. The change in resistances causes more current to flow through C1 and C2 and less current to flow through T1 and T2. Thus a potential difference is felt between the outputs or signal leads of the load cell. The gauges are mounted in a differential bridge to enhance measurement accuracy. When weight is applied, the strain changes the electrical resistance of the gauges in proportion to the load.

There are several common shapes of load cells that differ in their point of measurement of load and their fixed point, the implemented one for the device is a “Single point” or

"Cantilever" load cell with a maximum capacity of 20kg. This load cell is a straight block of material, fixed on one end, and loaded on the other, as shown on Figure 3.7.

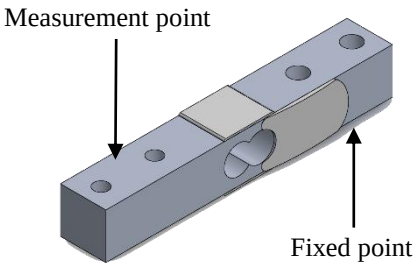

Figure 3.7. – Single Point Load Cell.

To measure the tangential force generated on each specimen, it was established on the design that each cell has to be installed directly to the stroke of each linear actuator. In order to do that, a configuration with a linear bearing was designed (**Figure 3.8**) so that the stroke can slide down to apply the load and at the same time the cell can measure friction when it is pushed by the stroke.

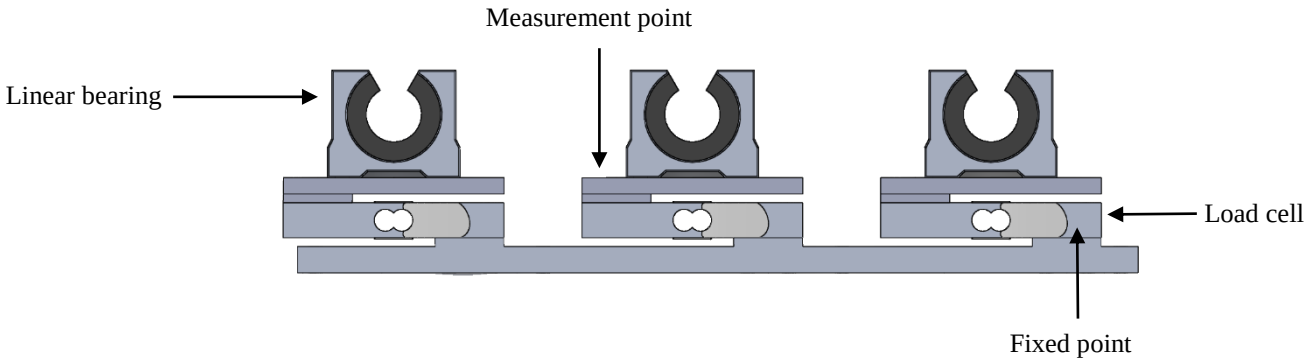

Figure 3.8. – Load Cell Configuration For Coefficient Of Friction Measurement.

3.2.4.2 Instrumentation amplifier. As mentioned in the previous section, the output signal of a strain gauge load cell, is in the order of millivolts, which means that the signal has to be conditioned to be readable and that is why an instrumentation amplifier is needed.

The instrumentation amplifier is one of the most useful, precise, and versatile available. It consist on three operational amplifiers and seven resistances (**Figure 3.9**).

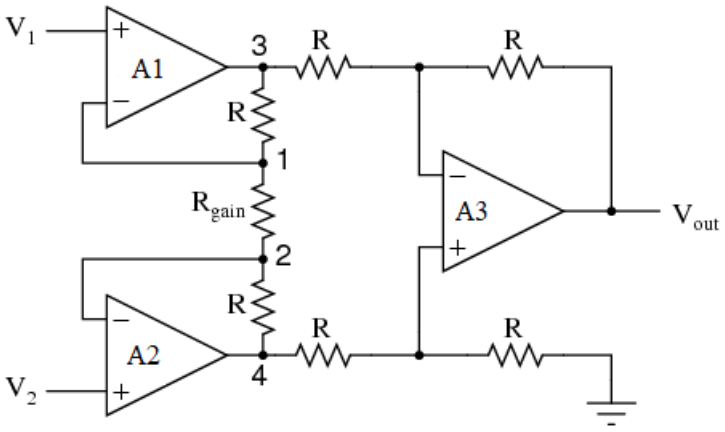

Figure 3.9. – Instrumentation Amplifier.

The operational amplifier A3 and the four equal resistances R connected to it, form a differential amplifier with a unitary gain. Just the resistance R_{gain} is variable in order to establish a gain according with the following relation:

$$\frac{V_{out}}{V_2 - V_1} = 1 + \frac{2}{a} \tag{1}$$

where:

$$a = \frac{R_{gain}}{R} \tag{2}$$

V_1 is connected to the negative input and V_2 is connected to the positive input. V_{out} is proportional to the difference between input voltages. Based on this statement, it was necessary to design an instrumentation amplifier for the load cells of the design. Considering that the rated output of the load cell is 1 mV/V and it voltage supply is 5 V, the output voltage range is from 0

to 5 mV. The ideal output would be a signal that oscillates between 0 and 5 V. To continue, the gain of the instrumentation amplifier must be calculated with the following equation:

$$G = \frac{V_{out}}{V_2 - V_1} \tag{3}$$

substituting values:

$$G = \frac{5\ V}{5\ mV} = 1000$$

The next step was to calculate the value of the equal resistances, using the gain value calculated, which mixing equations 1 and 3 results in the following equation:

$$G = 1 + \frac{2}{a} \tag{4}$$

solving for a the equation would be:

$$a = \frac{2}{G - 1} \tag{5}$$

substituting values:

$$a = \frac{2}{1000 - 1} = 2.002 \times 10^{-3}$$

If R_{gain} = 20Ω, then the value of R, can be calculated as:

$$R = \frac{R_{gain}}{a} \tag{6}$$

$$R = \frac{20\Omega}{2.002 \times 10^{-3}} = 9.99 \times 10^{3}$$

After solving the equations it is deduced that the next commercial available resistance value is 10 KΩ. The six resistances R, have a value of 10 KΩ, while the R_{gain} is a resistance of 20 Ω. The designed instrumentation amplifier is presented in **Figure 3.10**, where a low pass filter has been added to the output of the amplifier, to avoid noise and interferences that can affect the signal. A LM324 operational amplifier was selected because is one of the most common amplifiers, and less expensive than others.

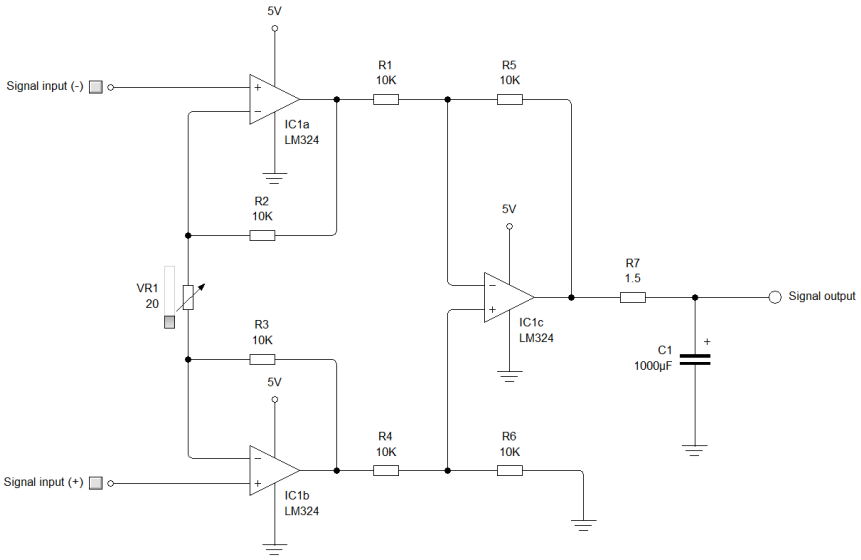

Figure 3.10. – Instrumentation Amplifier Designed.

The **c**uttoff frequency can be calculated as the following:

$$f_c = \frac{1}{2\pi RC} \tag{7}$$

substituting values:

$$f_c = \frac{1}{2\pi(1.5\Omega)(1000\mu F)} = 106.103\ Hz$$

3.2.5 Control system

Up to this section, the CNC-POD is composed by a motion system and a load system, each of them with different actuators and mechanisms to perform a specific task, for which a system that regulates the operation of each task is needed, and this is a control system.

A control system is divided in different stages, the controller is the stage which monitors and physically changes the operating conditions of a given dynamic system; the power stage conditions the signals emitted by the controller and at the same time it is an isolator between the controller and the actuator, the actuator is the physical system that needs to be controlled and the feedback stage is the measurement of the output signal to be compared with the input of the controller, in order to reduce errors in the control process.

According to the stages that conforms a control system, the control system designed for the CNC-POD includes the LabVIEW software and an Arduino microcontroller as the controller stage, the power stage is represented by electronic drivers for the stepper motors and electronic drivers for the linear actuators, and finally the feedback stage is composed by the load cells that measure the applied load by linear actuators and the load cells that measure the force generated in the stroke of each actuator.

3.2.5.1 LabVIEW Interface. LabVIEW (Laboratory Virtual Instrument Engineering Workbench) is a system – design platform and development environment for a visual programming language from National Instruments. Is commonly used for data acquisition, instrument control and industrial automation.

Programs developed in LabVIEW are called Virtual Instruments or VI's and its origin came from the control of instruments although nowadays it has expanded widely not only to the control of all types of electronics, but also to its embedded programming, communications, mathematics and more.

An interface or Virtual Instrument was designed in LabVIEW (**Figure 3.11**) to monitor and control the complete system, it has a section where the user can introduce input values, as the listed below :

1. Load (Newtons)
2. Pattern dimensions (millimeters)
3. Frequency (Hertz)
4. Location of the test on the specimen
5. Number of cycles
6. Start button
7. Stop button

Also, it can obtain output values during a test, as the listed below:

8. Enable Station button
9. Load feedback of each station
10. In vivo Coefficient of Friction graph
11. Cycles remaining
12. Completed cycles
13. Estimated time

Through this interface, users, can operate the device in an automatic way, they just have to introduce the desired parameter in which the test is developed, then press “Start” and the VI will automatically shows the estimated time of the complete test, the device will start to work and the user will just have to wait until the test ends.

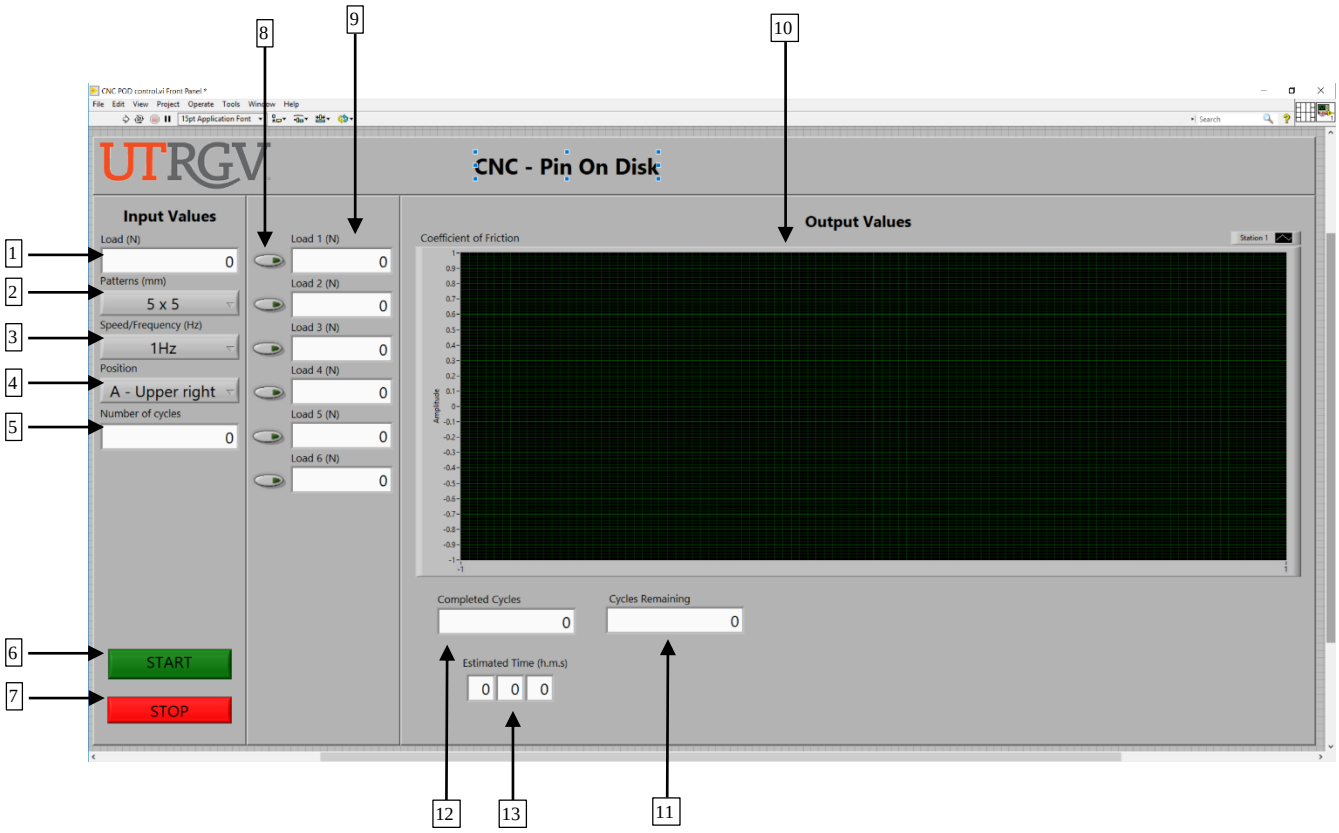

Figure 3.11. – LabVIEW Interface (Virtual Instrument).

The second stage in the control system is the control electronics, this is a set of electric drivers, transducers, and amplifiers connected to a data acquisition card which is communicated with LabVIEW in order to the device execute the desired functions.

3.2.5.2 Arduino Mega 2560. Starting with the data acquisition card, an Arduino Mega 2560 was chosen to act as a DAQ (Data Acquisition card), mainly because of its wide capacity of inputs and outputs both digitals and analogic, which allows to operate all the mechanisms of the device with the same microcontroller. It is important to clarify, that the control process is completely executed from LabVIEW, and the Arduino is just a medium to communicate software with the device. A picture of the Arduino Mega 2560 is shown in **Figure 3.12**.

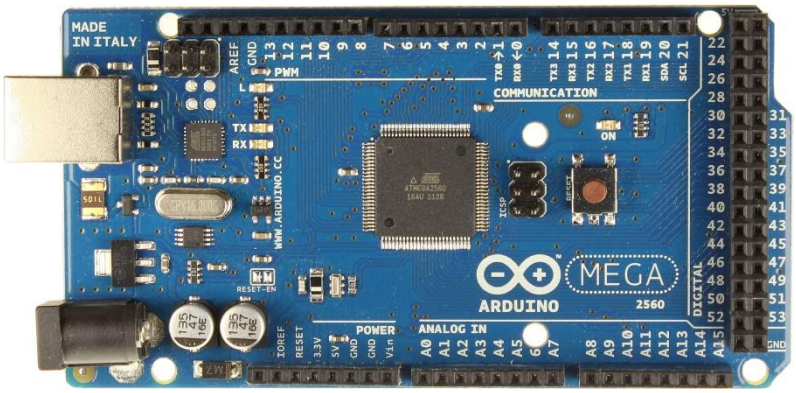

Figure 3.12. – Arduino Mega 2560.

3.2.5.3 Micro step driver M542T. Drivers are connected to the Arduino. Drivers are power electronic circuits that isolate the main control circuit from the actuators or motors, this is a power stage that amplifies the control signals emitted by the controller and applies the amplified signal to the actuator and prevents damages in the controller giving to the actuator all the power needed, regulating voltages and currents. The M542T is a micro step driver that allows the interaction and control of a stepper motor, based on pure-sinusoidal current control technology. A picture of the M542T is a micro step driver is shown in **Figure 3.13**.

Figure 3.13. – Micro Step Driver M542T.

The driver receives two digital input signals from the Arduino, the first one for move a step, and the second one for the direction of the step. **Table 3.3** shows the electrical specifications of the M542T driver.

Table 3.3. - Driver M542T Electrical Specifications.

Supply Voltage (V)	24 – 50
Output Peak Current (A)	1.5 - 4.5 (3.0 RMS)
Logic Signal Current (mA)	7 – 16
Pulse Input Frequency (Hz)	0 – 300 K

3.2.5.4 DC Motor driver VNH5019 for linear actuators. The Driver VNH5019 operates from 5.5 to 24 V and can deliver a continuous 12 A (30 A peak). It works with 2.5 to 5 V logic levels, supports ultrasonic (up to 20 kHz) PWM, and features current sense feedback (an analog voltage proportional to the motor current). Along with built-in protection against reverse-voltage, over-voltage, under-voltage, over-temperature, and over-current.

The following diagram (**Figure 3.14**) shows the minimum connections required for interfacing this motor driver with a microcontroller:

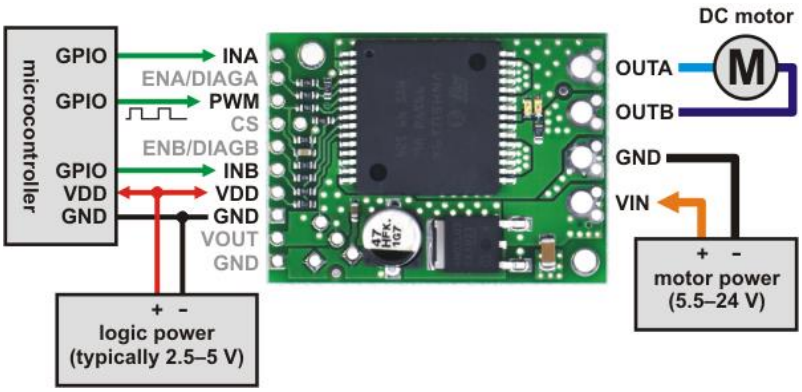

Figure 3.14. – DC Motor Driver VNH5019.

One driver is implemented for each linear actuator in order to control the sliding speed of them, with the purpose to manage the load that is going to be applied on the specimen. As shown in the **Figure 3.14** the driver receives three input signals, one is the PWM to control the speed of the actuator, while the other two controls the direction of the displacement.

Up to this point, the design of the systems that integrates the CNC-POD has been described with all their components separately, but finally, the complete physical design is presented in **Figure 3.15,** where all the parts of the device are assembled.

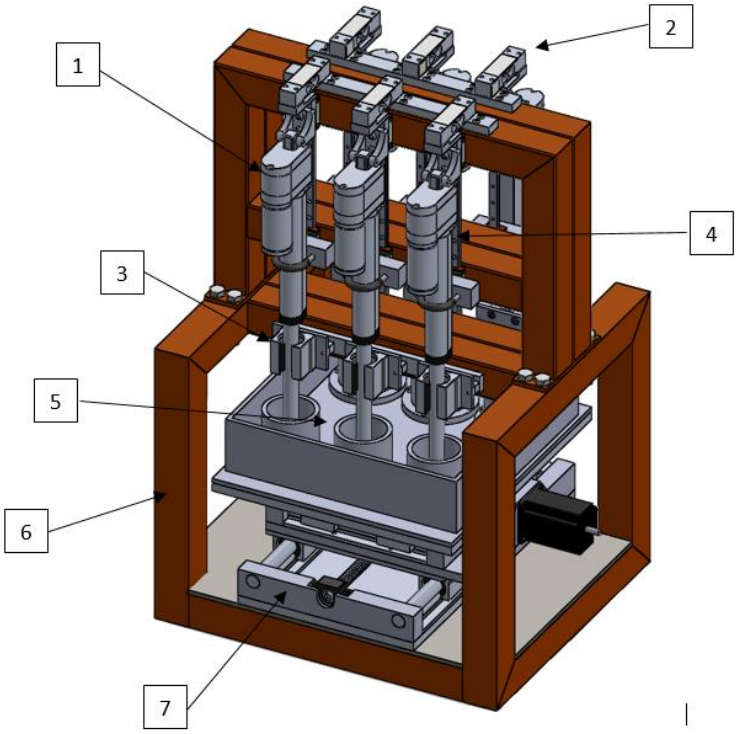

1. Electric linear actuator
2. Load cell sensor
3. Rail guide for stroke with load cell sensor
4. Rail guide for actuator housing
5. Disk holder with lubricant container
6. Main frame of the device
7. XY (CNC) table

Figure 3.15. – Final Design Of The Bidirectional Wear Testing Device CNC-POD.

In addition to the physical design, an electrical schematic design presented in **Figure 3.16** establishes connections between the electrical components of the CNC-POD. A computer running the LabVIEW VI is connected to the Arduino Mega 2560, this microcontroller receives feedback from the load cells through its analog inputs, previously conditioned by the instrumentation amplifier, while it sends the control signals to the microstep drivers and the actuator drivers through its digital outputs. The complete system is powered by two DC sources, one of 24 V (stepper motors) and the other one of 12 V (linear actuators, load cells).

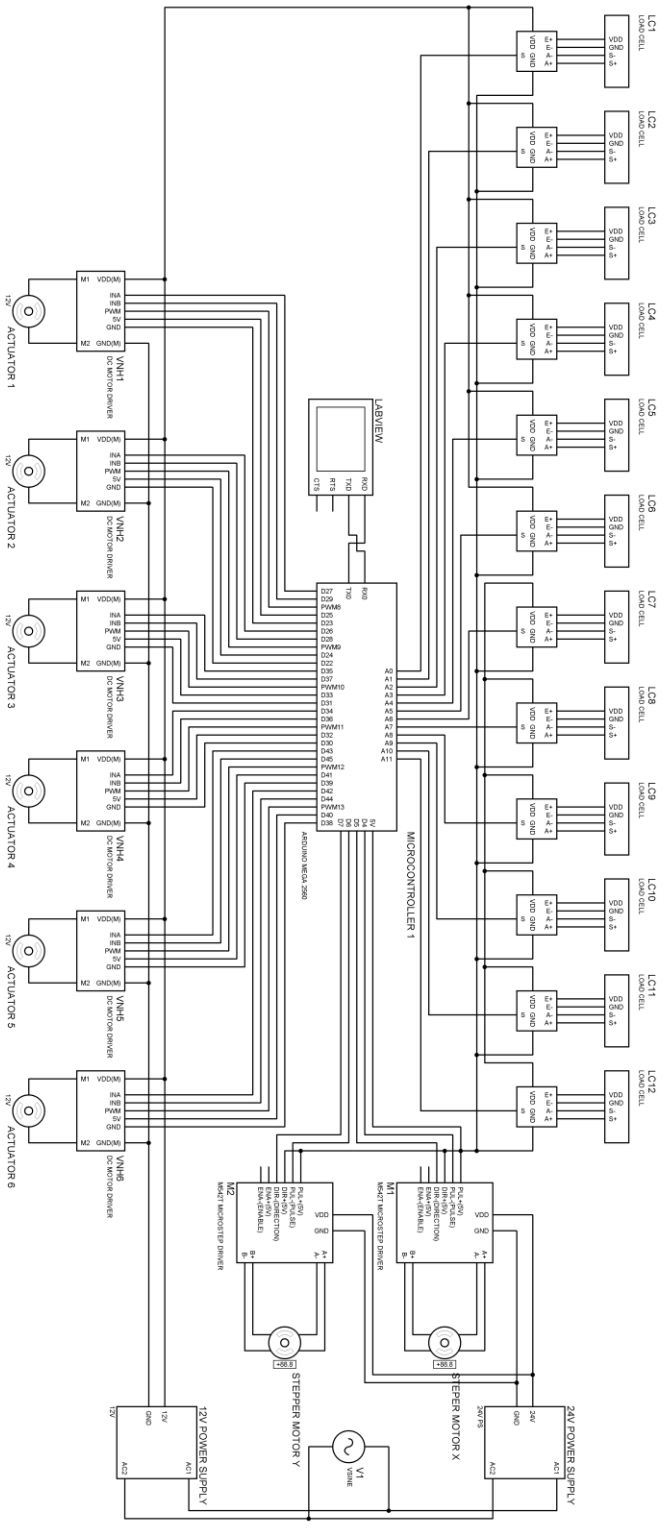

Figure 3.16. – General Schematic Of The Designed Control System.

CHAPTER IV

EXPERIMENTAL PROCEDURE AND FABRICATION

4.1 Introduction

As a part of the learning and acquisition of knowledge, it is necessary to include the experimental part with the purpose of giving support and reliability to the theoretical part of any specific topic. At present, most of the experimental sciences are supported by technology that allows them to have different tools on hand to facilitate the study of specific situations.

During this chapter, the fabrication process of the designed device is described following all the procedures and activities required to build the device.

4.2 Fabrication of a first Prototype (Single station)

Before to start building the designed device, it was necessary to verify that systems and their components assembled together were working on the desired way, for this reason a single station with a basic structure was developed.

4.2.1 Building the structure

First of all, the structure was made of rectangular tube welded as a frame with four supports inclined 45° and then it was screwed to a 0.25-inch thickness steel plate, where the rest of the components were going to be assembled.

a) **b)**

Figure 4.1. – (a) Front And (b) Isometric Views Of The Structure For The First Prototype.

4.2.2 Manufacture of parts on lathe and milling machine

During the fabrication process, some parts were manufactured with the lathe and the milling machine on the machine shop, as shown in **Figure 4.2**.

Figure 4.2. – Aluminum Piece, Manufactured On A Milling Machine.

4.2.3 Components assembly

After the frame structure was completed, all the components for a single station where assembled to it and after that, the first prototype was tested as shown in **Figure 4.3**.

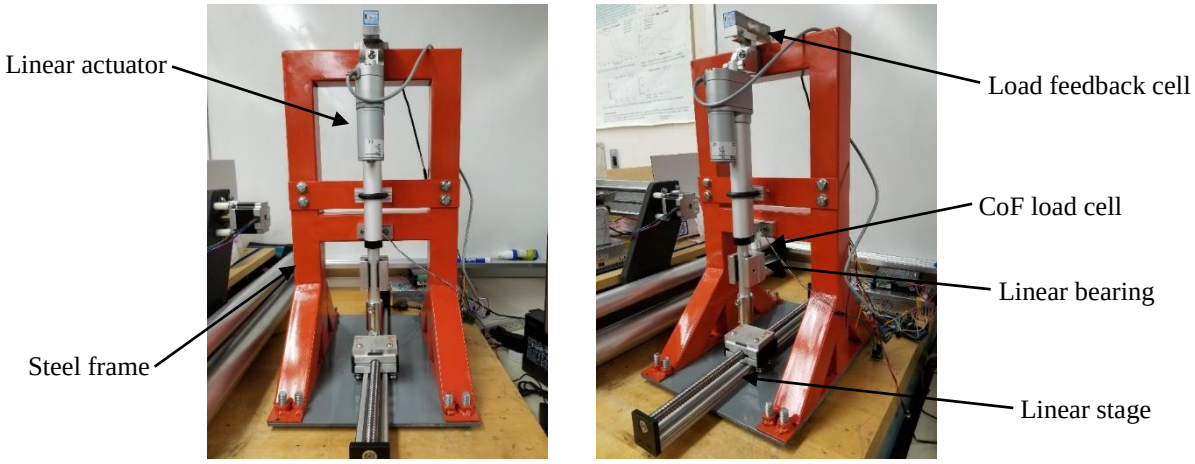

a) **b)**

Figure 4.3. – (a) Front And (b) Isometric Views Of The Finished First Prototype.

4.3 Fabrication of the CNC – POD

After verifying the performance of the different systems working together on the first prototype, the fabrication of the CNC-POD began.

4.3.1 Building the structure

The first step of the development of the device was the construction of the complete frame of the device. After analyzing the results obtained in the first prototype it was decided to change the thickness of the wall of the rectangular tube from 0.0625-inch to 0.125-inch in order to obtain better results when the system is applying load during test.

a) **b)**

Figure 4.4. – (a) Front And (b) Isometric Views Of The Frame Of The CNC-POD.

4.3.2 Manufacture of parts on lathe and milling machine

Just like in the first prototype, some parts of the designed device were manufactured on the milling machine or in the lathe and all this process was carried out in the machine shop. Some of the manufactured parts are listed below:

- X-Y Table, made on aluminum
- Mounts for load cells, made on aluminum
- Pin holder, made on stainless steel
- Specimen chambers, made on stainless steel
- Container of specimen chambers, made on stainless steel

4.3.3 X-Y Table Assembly

As a third step, the X-Y table was developed, using aluminum plates of .25, 0.5, 0.75, and 1-inch in thickness. The two stages (X and Y axis) were built as shown in **Figure 4.5** and **Figure 4.6**.

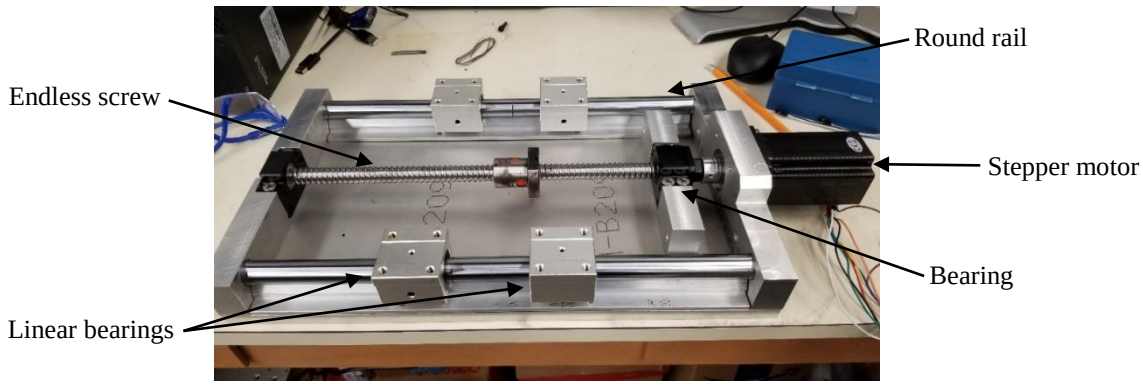

Figure 4.5. – X-Axis Stage Of The Motion System, Manufactured In Aluminum.

The x-axis stage is the longest one in the XY table for two reasons, the first one is because this mechanism carries out the longest route in the device, and the second reason is because when it is necessary to install or remove the sample before or after the test, it is necessary to place the samples away from the linear actuators.

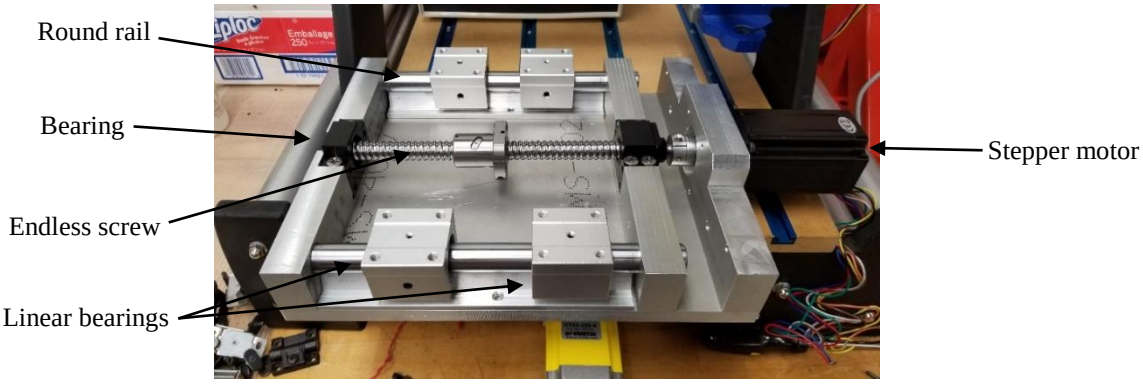

Figure 4.6. – Y-Axis Stage Of The Motion System, Manufactured In Aluminum.

The y-axis stage is shorter, it carries out a route of 5 mm maximum, this stage is mounted above the x-axis stage (as shown on **Figure 4.7**) in order to produce de bidirectional motion when both of them are operating.

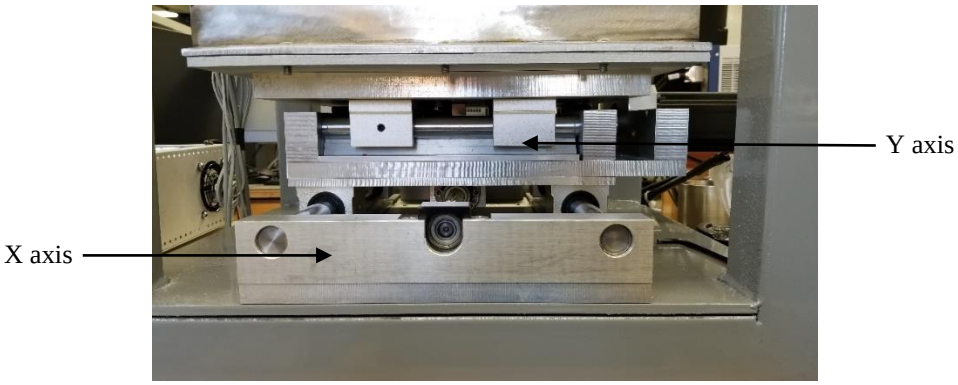

Figure 4.7. – X-Y Table Completely Assembled.

4.3.4 Specimen chambers container assembly

After manufacturing all the parts of the specimen chambers the containers, those components were assembled and mounted on the X-Y table. Following the design presented before, **Figure 4.8** shows the specimen chambers mounted on the container.

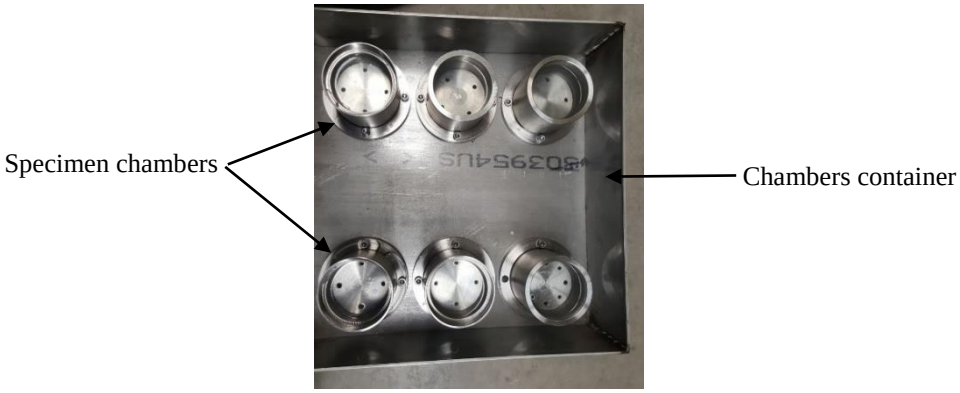

Figure 4.8. – Specimen Chambers Mounted On The Chambers Container.

4.3.5 Load modules assembly

Continuing with the fabrication process, the next step was to assembly the linear actuators, each actuator was mounted to a linear bearing and a load cell located above the actuator, to measure the load applied by the actuator (**Figure 4.9**).

Figure 4.9. – Load Cell Mounted Above The Linear Actuator.

Then, the complete set of linear actuators and load cells was mounted to the structure, following the original design (**Figure 4.10**).

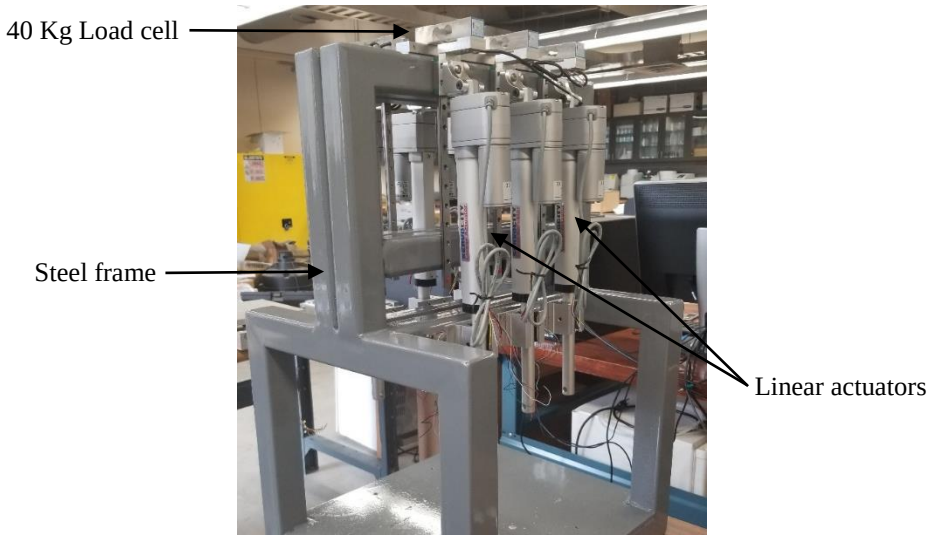

Figure 4.10. – Linear Actuators Mounted On The Structure To Conform The Load System.

4.3.6 Assembly of the CNC-POD

After mounting most of the components of the device together, it was time to complete the assembly, installing the loads cells for coefficient of friction measurement in the strokes of the linear actuators (**Figure 4.11**). Then, the X-Y table with the chambers container was installed on the structure under the linear actuators (**Figure 4.12**), and each pin holder was assembled to the stroke of a linear actuator (**Figure 4.13**).

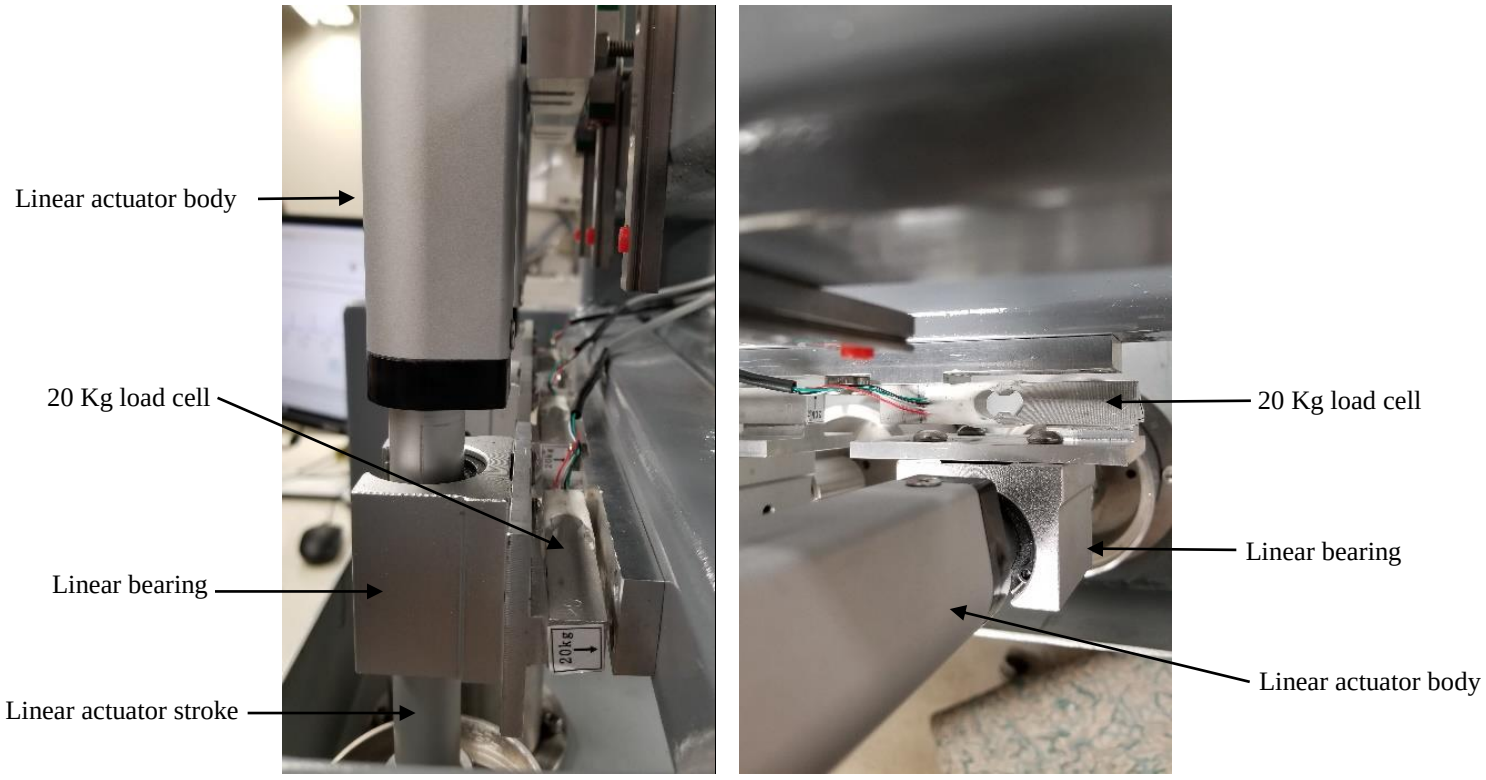

a) **b)**

Figure 4.11. – (a) Sided View Of The Cof Load Cell, (b) Top View Of The Cof Load Cell.

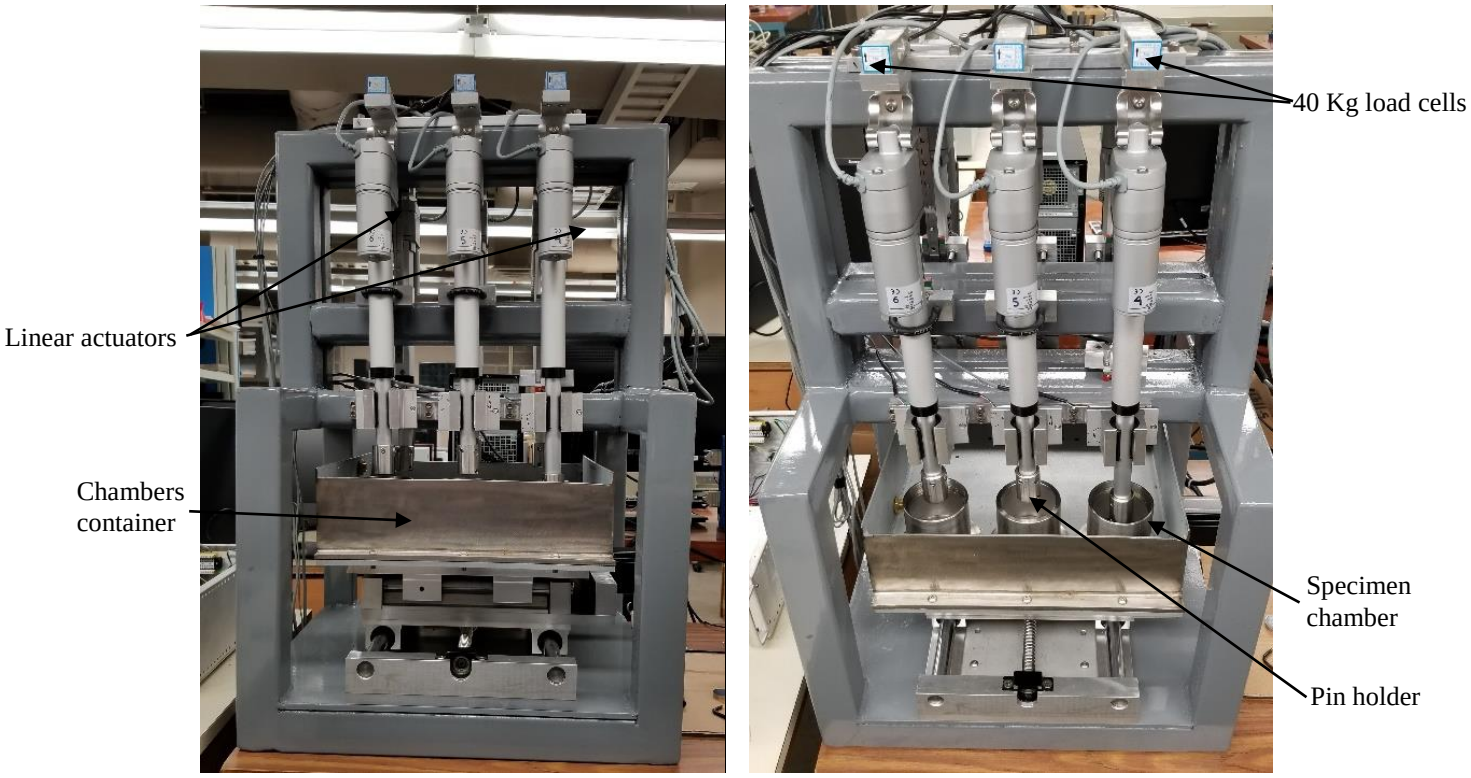

a) **b)**

Figure 4.12. – (a) Front View Of The CNC-POD, (b) Top View Of The CNC-POD.

Figure 4.13. – Pin Holder Installed On Each Linear Actuator.

4.3.7 Control cabinet assembly

To complete the fabrication process, a control cabinet was assembled. First, the power supplies and drivers were connected to the Arduino, as shown in **Figure 4.14.**

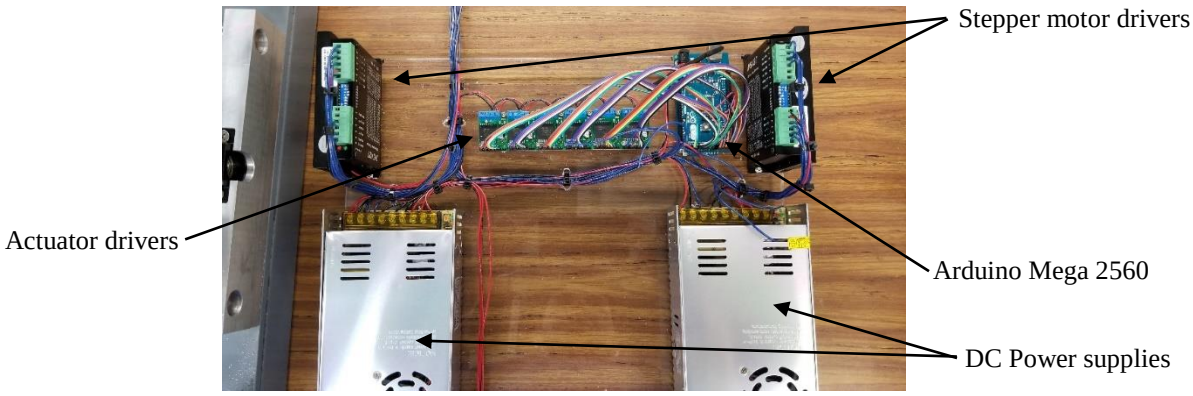

Figure 4.14. – Power Supplies And Drivers Connected To The Arduino.

Then all the circuits were mounted in the cabinet and wired to the external connectors and the front buttons to complete the fabrication process of the CNC-POD (**Figure 4.15**).

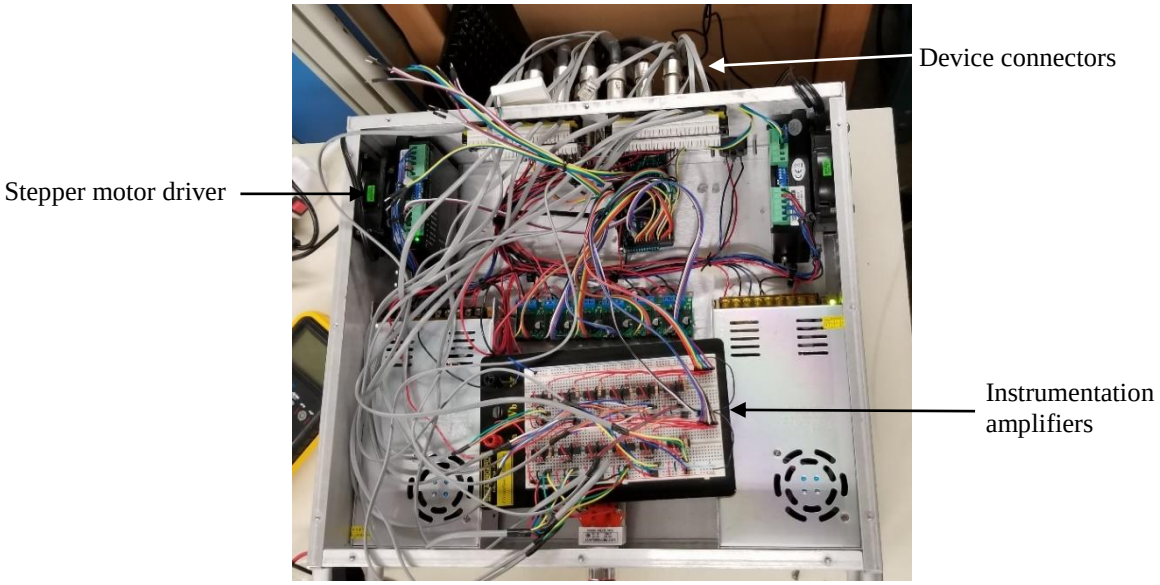

Figure 4.15. – Control Cabinet Assembled.

4.3.8 Load cells Calibration

Once everything was installed and connected, the next step consisted on the calibration of load cells. The first step to calibrate the load cells was to verify that the output voltage from the amplifiers increases when a small force is applied to the cell, then by placing known weights on each cell, voltage differences were recorded in order to establish a proportional scale between the read values and the known values, see **Figure 4.16**. For this process, an independent virtual instrument was created on LabVIEW, where the reading is shown in volts, kilograms, pounds and newtons, in **Figure 4.17**.

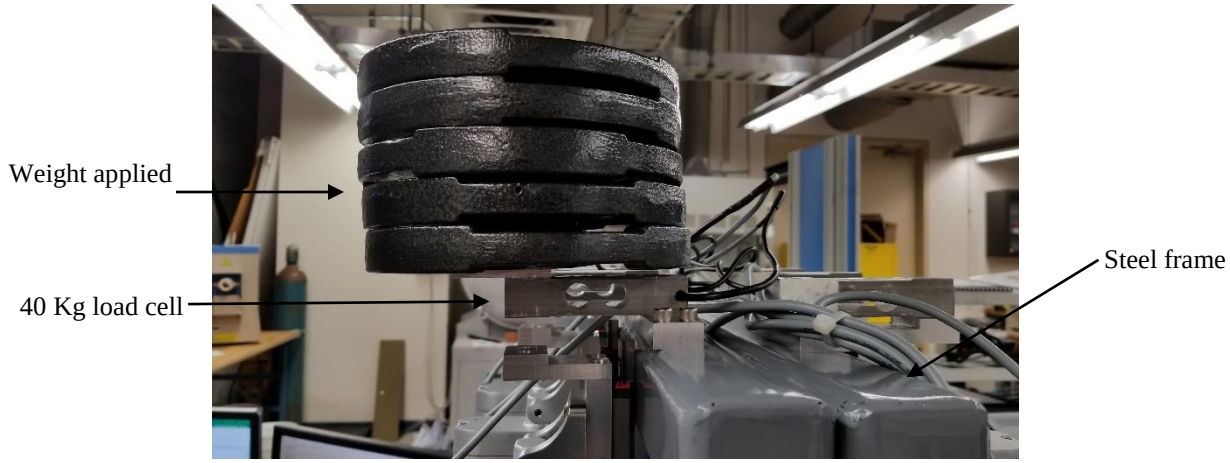

Figure 4.16. – Load Applied To A Load Cell For Calibration.

The calibration procedure consisted on applying a previous measured weight on each load cell and measure the increase of voltage, this in order to define the relation between the applied weight and the output voltage which operates on a range from 0 to 5 volts. The **Table 4.1** shows the recompilation of calibration values.

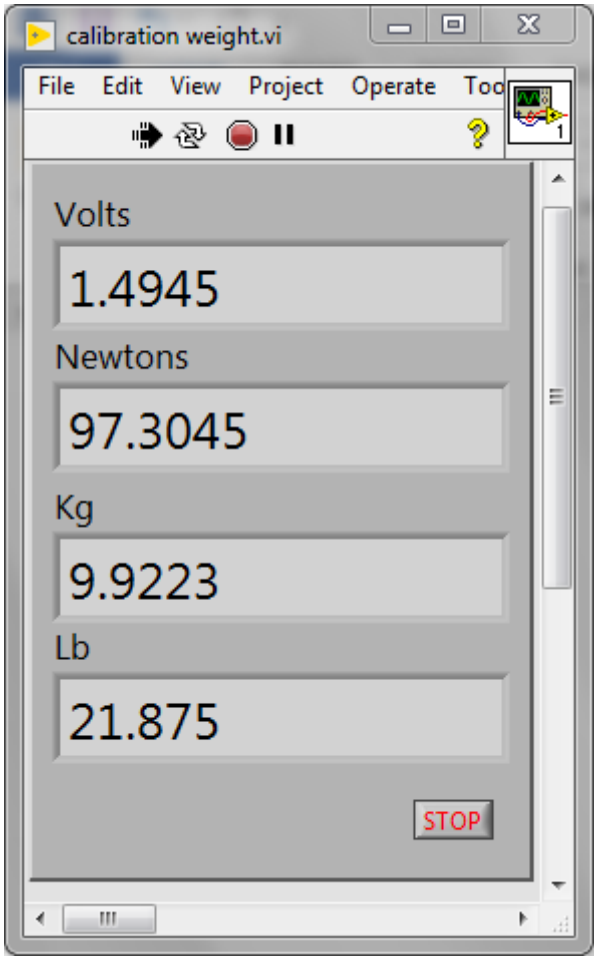

Figure 4.17. – Labview Virtual Instrument For Load Cell Calibration.

Table 4.1. – Load Cell Calibration Values

Kg	Voltage					
	Load cell 1	Load cell 2	Load cell 3	Load cell 4	Load cell 5	Load cell 6
1.998641	0.5194	0.4802	0.5096	0.5030	0.3773	0.1666
3.983108	1.0192	0.9849	1.0143	1.0061	0.8918	0.6713
5.9534	1.5337	1.4798	1.5337	1.5157	1.4063	1.1662
7.937866	2.0384	2.0041	2.0384	2.0269	1.9404	1.7003
9.915245	2.5529	2.5284	2.5529	2.5447	2.45	2.205
11.89404	3.0772	3.0086	3.0527	3.0461	2.9547	2.7097
13.87284	3.5721	3.5231	3.5476	3.5476	3.4741	3.2242

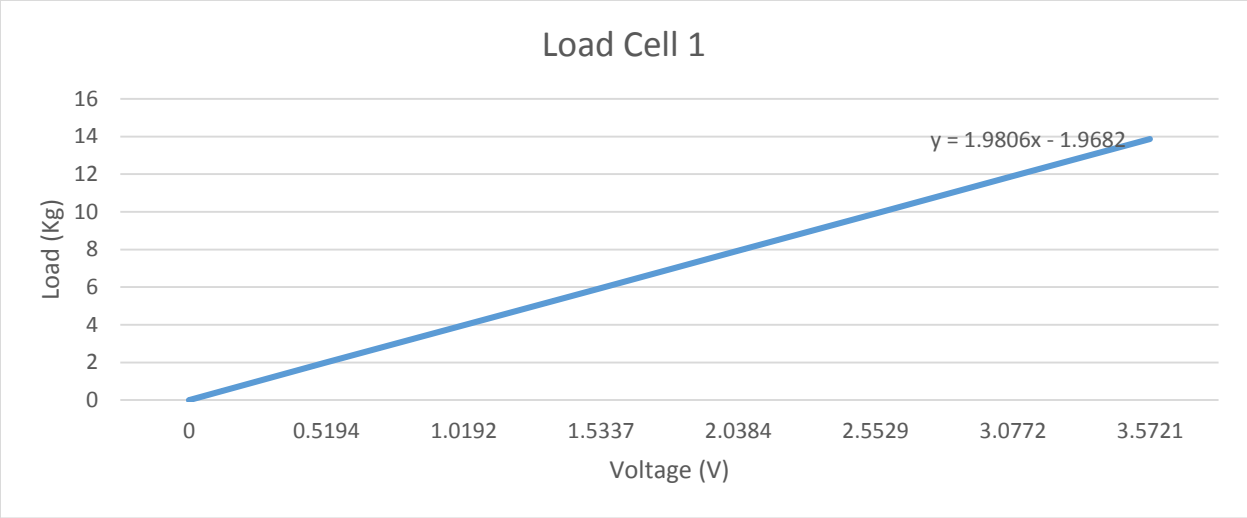

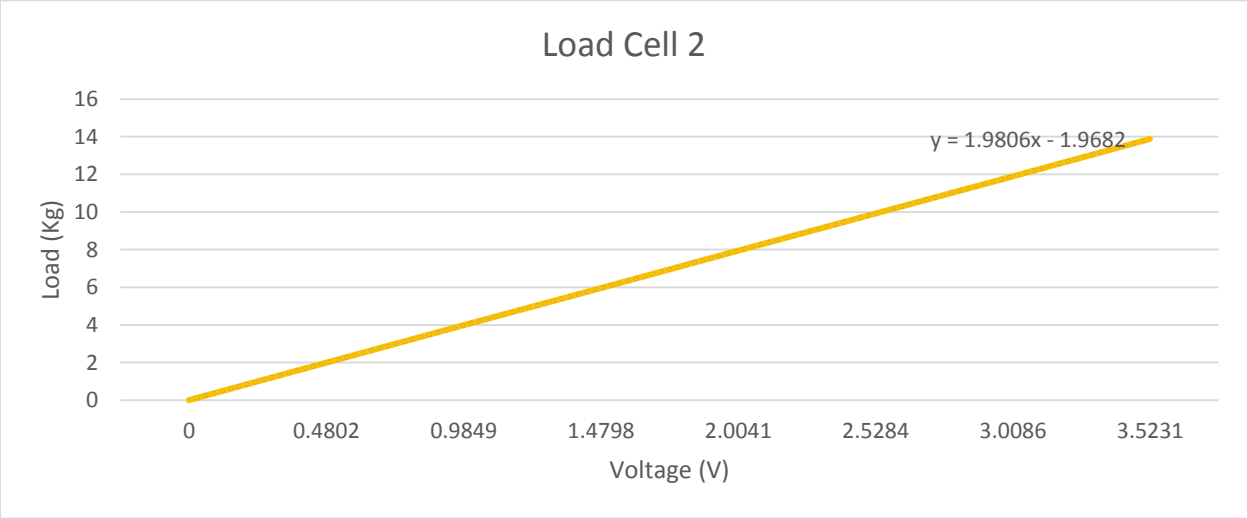

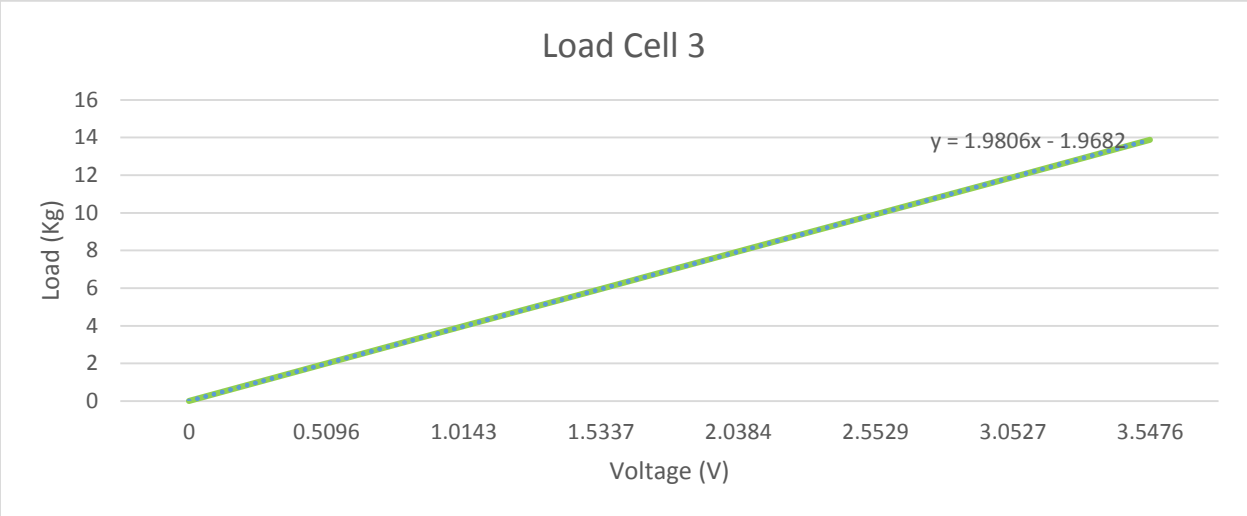

Figure 4.18 Calibration Graphs Of Load Cells 1, 2 And 3.

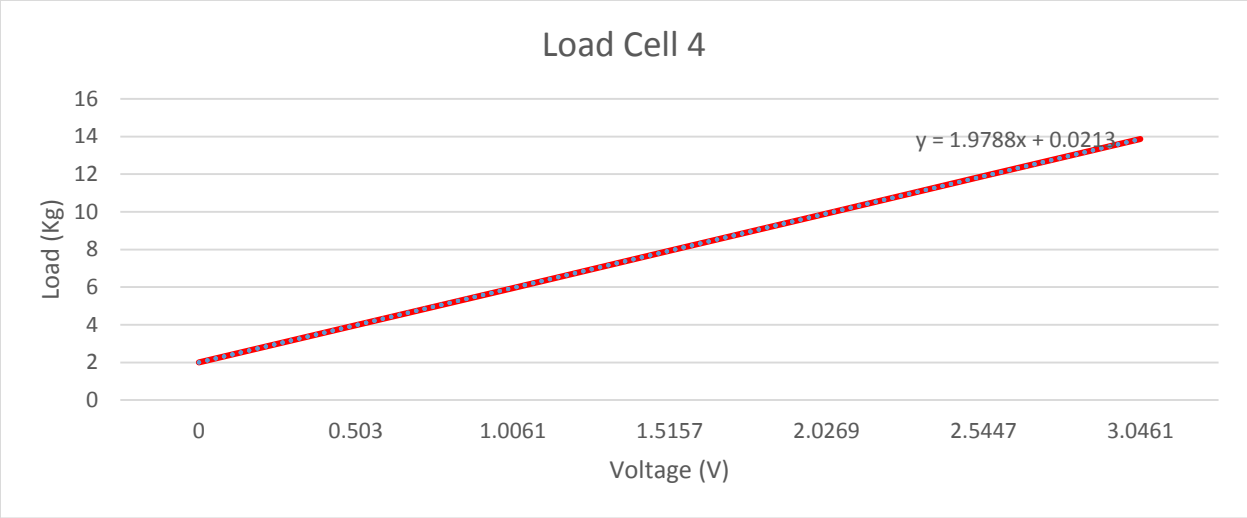

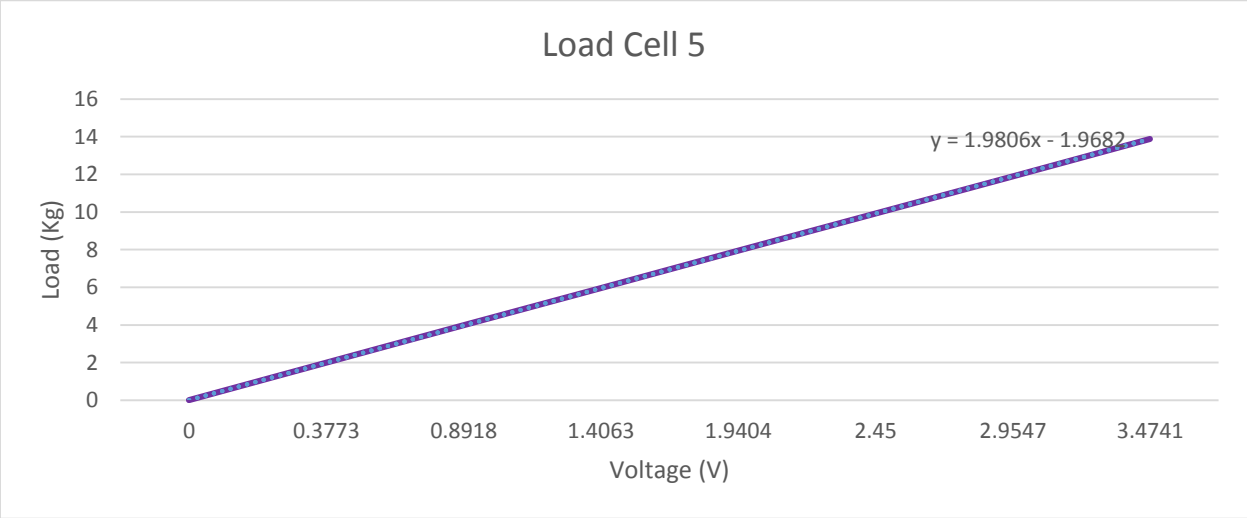

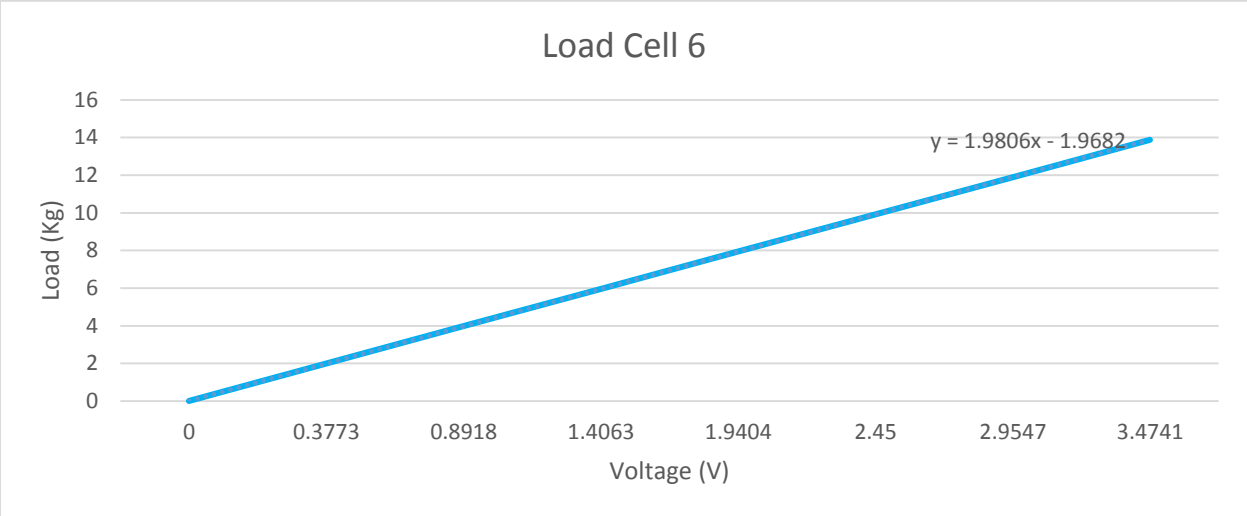

Figure 4.19 Calibration Graphs Of Load Cells 4, 5 And 6.

4.4 Validation tests

After the fabrication process was completed, validation tests were carried out on the CNC-POD, in order to validate its performance. Friction and wear tests were carried out using a ball-on-disc configuration under unlubricated conditions. The disc used during the tests was a CoCrMo alloy disc (ASTM F1537-11) commercially known as Micro-Melt Biodur CCM Plus with 1.125 inches in diameter and 0.25 inches in thickness. Disc was polished to implant grade surface smoothness, with a centerline roughness of 0.015 μm. In order to concentrate all the wear on the disc, a hardened AISI 52100 bearing steel ball with 0.375 inches in diameter was used as a stationary counter body. The measured hardness was 44 and 60 HRC for the disc and the steel ball respectively. CoCrMo alloy disc and the steel ball are shown on **Figure 4.18**.

Figure 4.20. Cocrmo Alloy Disc And Steel Ball Used During The Wear Tests.

Four different articulation patterns including a 5 mm x 5 mm, 4 mm x 6 mm, 3 mm x 7 mm, and 0 mm x 10 mm were digitalized into the CNC-POD. Four wear tests were performed on the CNC-POD using the four different patterns. Each wear test was carried out using one of the four patterns at a frequency of 1 Hz during 1000 cycles with a constant applied load of 25 N or an

applied stress of 1.12 GPa, which corresponds to the yield strength of the CoCrMo alloy. The coefficient of friction was monitored during each wear test. Figure 4.19 shows the specimens mounted on the CNC-POD. The wear tests using the 4 mm x 6 mm were repeated using a constant load of 225N.

Figure 4.21 Specimen Mounted On The CNC-POD Before The Wear Tests.

CHAPTER V

RESULTS

5.1 Introduction

Once fabrication and experimentation processes of the CNC-POD are completed, a compilation of results is needed in order to compare and validate the obtained results with the desired results.

5.2 Device functionality

At this point it is important to remember that the main objective of this project was to design and develop a wear testing device capable to generate motion in two dimensions to study the effect of the cross-shear phenomena in the wear of materials, and also it can be used to perform different types of wear tests. In the present chapter, a summary of the results of the CNC-POD operation and performance are presented, based on the validation tests described on the previous chapter.

5.2.1 Motion system

As described on section 3.2.2.1, the motion system was composed by two stepper motors that drive motion on two perpendicular linear stages. In order to obtain a specific displacement on each linear stage, a certain number of pulses has to be sent to each stepper motor, as shown in

Figure 5.1, in which the control signals for the stepper motors describes the motion pattern of 5mm x 5 mm.

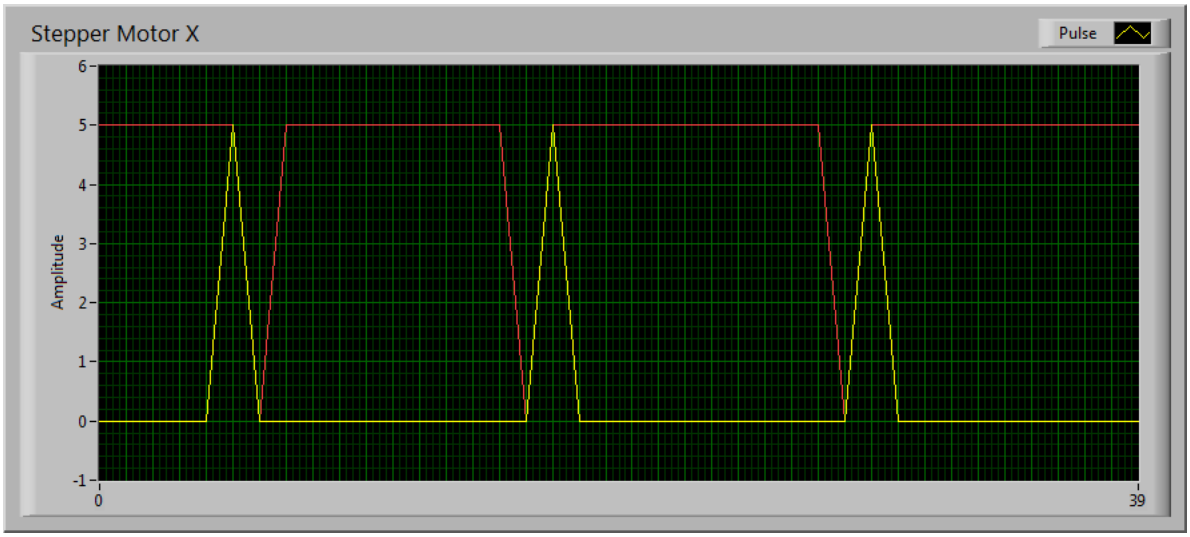

a)

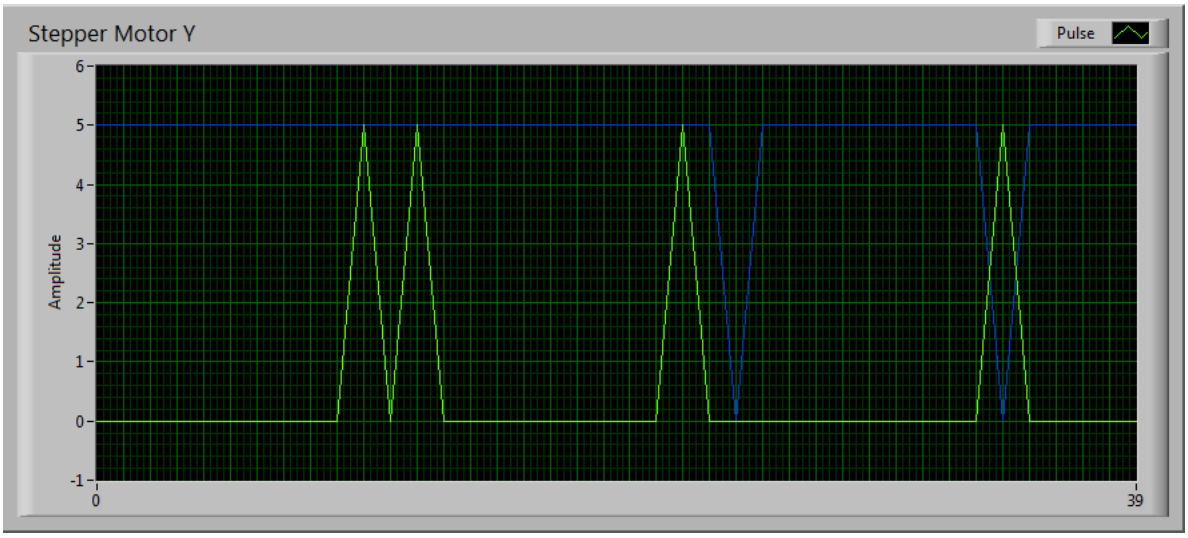

b)

Figure 5.1. – (a) Control Signals For Stepper Motor X, (b) Control Signal For Stepper Motor Y For A Pattern Of 5mm X 5mm.

Figure 5.2 shows the CoCrMo alloy disc after the wear test. The wear track corresponding to the four different patterns (5 mm x 5 mm, 4 mm x 6 mm, 3 mm x 7 mm, and 0 mm x 10 mm) can be observed on the disc surface after the wear tests. Also, it can be seen that a single specimen or disc can be used to perform four tests, placing each test on a different quadrant of the specimen or disc. This innovation allows us to save material, performing four tests per disc.

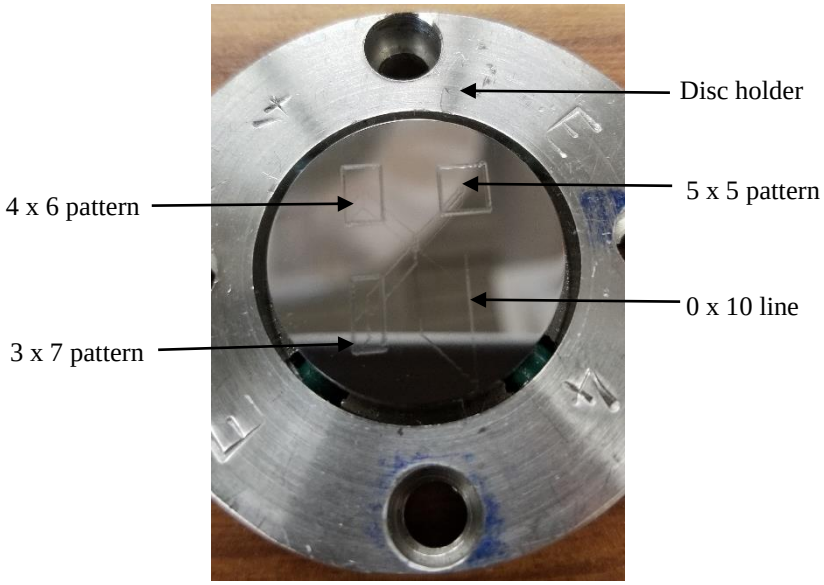

Figure 5.2. – Wear Patterns After Wear Testing.

5.2.2 Load System

The load system described on section 3.2.3.1 presented a mechanism composed by six linear actuators capable of applying loads up to 500N, those actuators have two ways of feedback, one is the position feedback which operates through a potentiometer inside the actuator, and the other one is the load cell (with a maximum capacity of 40 kg) installed above

each actuator. **Figure 5.3** shows the relation between the speed of the actuators and position, while **Figure 5.4** shows the load application by the actuator.

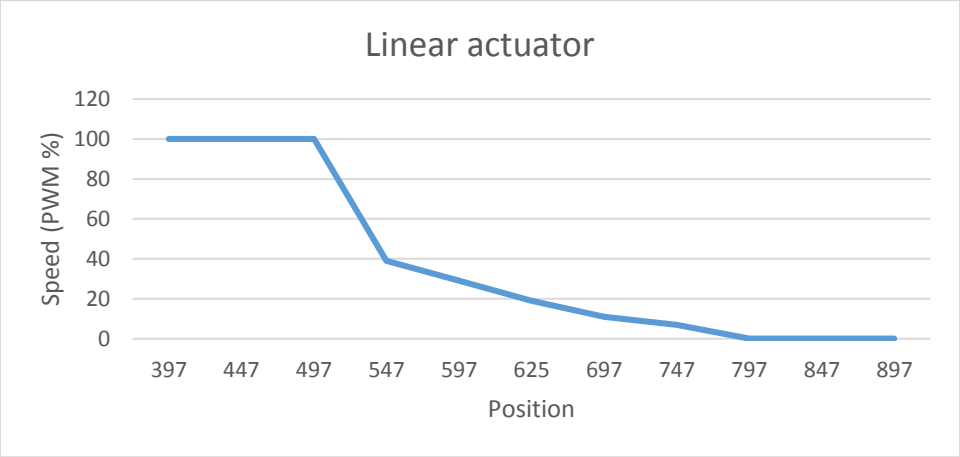

Figure 5.3. – Relation Between The Speed Of The Actuator And It Position.

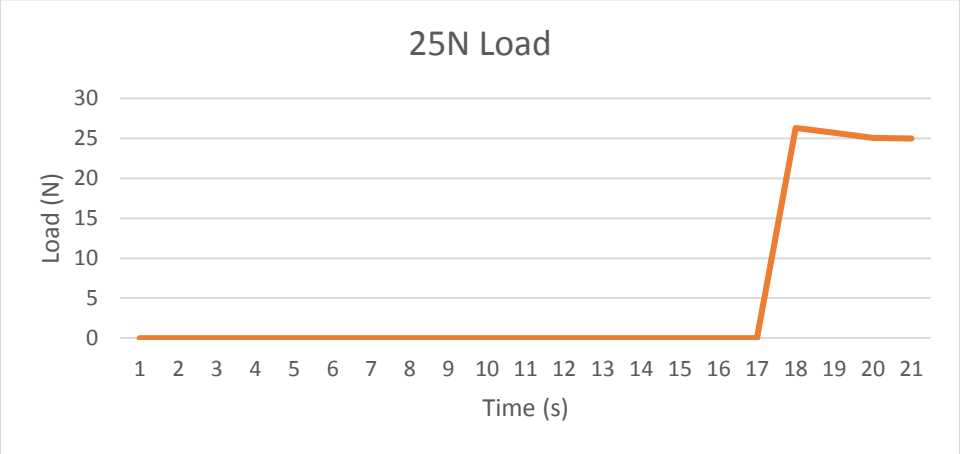

Figure 5.4. – Relation Between Applied Load And Time.

5.2.3 Coefficient of friction calculation

Following the requirements and parameters established in the Standard Test Method for Linearly Reciprocating Ball-on-Flat Sliding Wear (ASTM G133-95), tests were performed on

the CNC-POD applying two different constant loads (25 and 225N) in order to verify the performance coefficient of friction calculation. The coefficient of friction was calculated by LabView diving the tangential force (monitored by the CoF load cell with 20 kg maximum capacity) by the normal load measured with the load cell located above the linear actuator. The coefficient of friction was calculated from:

$$\mu = \frac{F}{N}$$

Where μ is the coefficient of friction, *F* is the tangential force, and *N* is the normal force applied to the specimens.

5.2.3.1 Test using 25 Newtons of load. The first test was performed with a load of 25N, in a frequency of 1 Hz, sliding on a square pattern of 5mm x 5mm, with a total distance of 20 mm per cycle, without lubrication. **Figure 5.5** show the graphic of the calculated coefficient of friction read from LabVIEW, while **Figure 5.6** shows the same graphic plotted with the numeric values read from load cells.

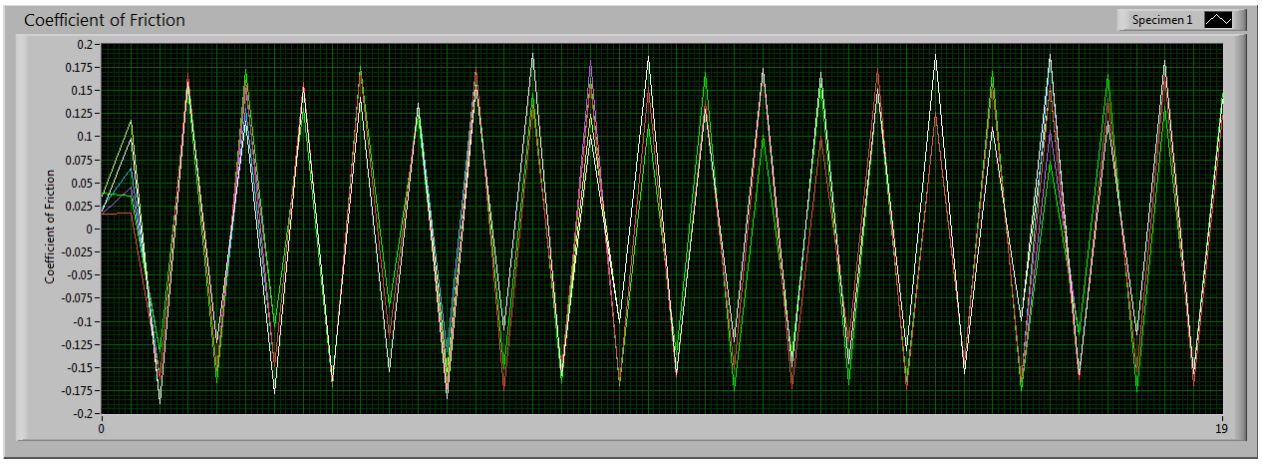

Figure 5.5. – Coefficient Of Friction Calculated With Labview With A Load Of 25N.

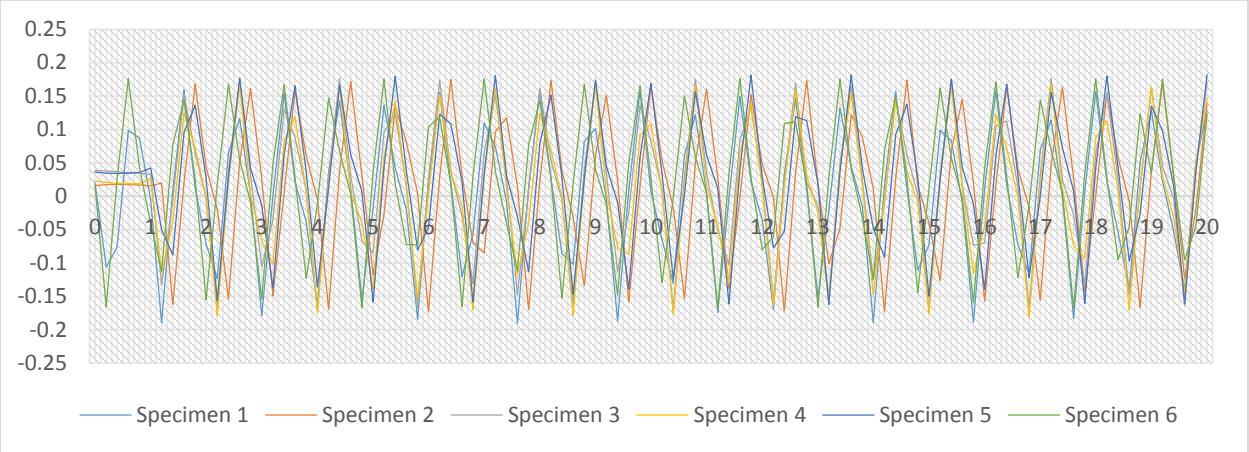

Figure 5.6. – Coefficient Of Friction Calculated With Values Read From Load Cells, With A Load Of 25N.

5.2.3.2 Test using 225 Newtons of load. Another test was performed with a load of 225N, a frequency of 1Hz, sliding on a rectangular pattern of 6 mm x 4 mm with a total distance of 20 mm per cycle without lubrication during 1000 cycles. **Figure 5.7** show the graphic of the calculated coefficient of friction read from LabVIEW, while **Figure 5.8** shows the same graphic plotted with the numeric values read from load cells.

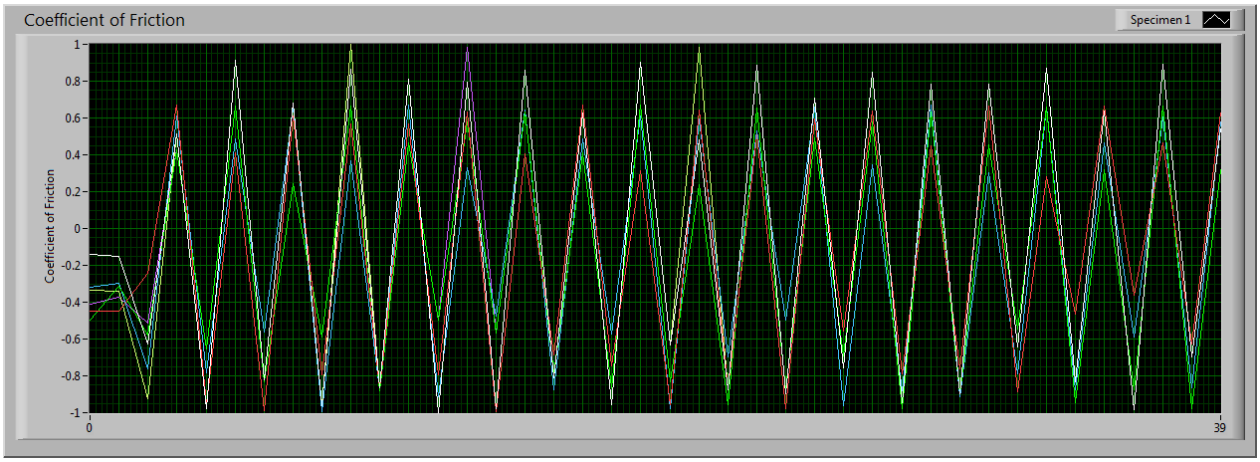

Figure 5.7. – Coefficient Of Friction Calculated With Labview With A Load Of 225N.

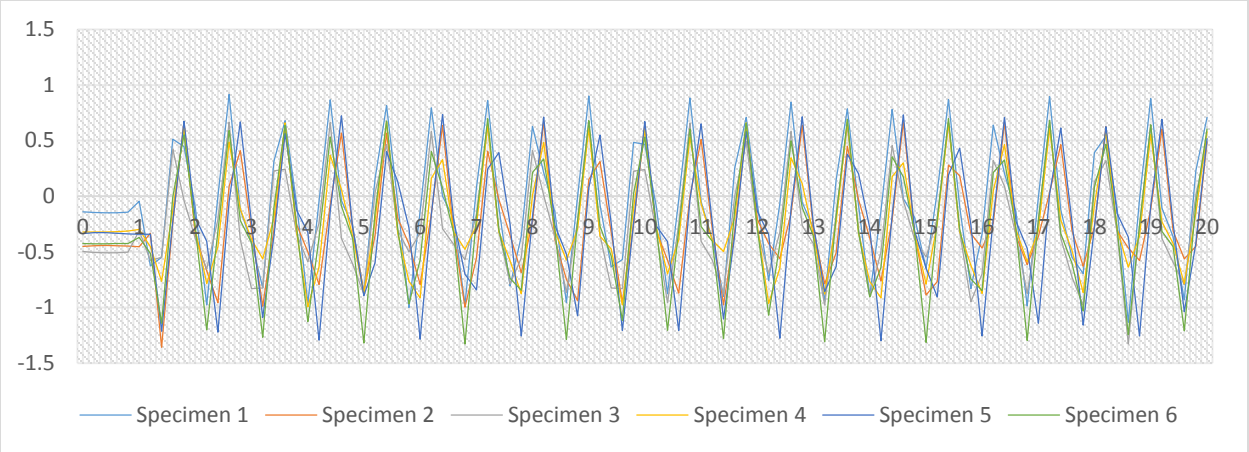

Figure 5.8. – Coefficient of Friction Calculated with Values Read from Load Cells, with a Load of 225N.

From the results of the coefficient of friction, it can be observed that as the normal force increases, the coefficient of friction increases. This was confirmed using the 25 N and 225 N loads.

CHAPTER VI

CONCLUSIONS AND FUTURE WORK

6.1 Conclusions

In the present project, a wear testing device denominated CNC-POD capable to reproduce wear patterns in two axes allowing the study of the "cross-shear" effect on the wear of materials was successfully designed and manufactured. Based on the experimental results, the following main conclusions can be drawn:

- The X-Y table included in the motion system allows the device to reproduce a wide range of two dimensional patterns in the millimeter scale under a specific load.
- A maximum load of 500 Newtons (112 pounds) can be applied to each testing station through linear actuators, which can be programed individually.
- The CNC-POD is capable to measure friction force during testing, and the coefficient of friction can be calculated on each testing station.
- Motions and loads are fully programmable through LabView.
- Six testing stations were included in the design of the CNC-POD in order to perform up to six wear tests simultaneously.

With the development of this system, it is possible to simulate both unidirectional and bidirectional sliding motions between the contact surfaces and measure the combined effect of

multidirectional motion and different loads in lubricated environments, allowing a more accurate replication of in vivo conditions for biomaterials. Also, with the characteristics of the CNC-POD, it is possible to perform wear tests following the specifications included in different standards such as ASTM F732, ASTM G133, and ASTM G99.

6.2 Future work

The future work includes a comprehensive validation of the device, performing different tests following the specifications included the different ASTM standards mentioned before, and including all the features of the CNC-POD described on this document.

REFERENCES

Bragdon, C., O'Connor, D., Lowenstein, J., Jasty, M., Biggs, S., & Harris, W., (2001) "A New Pin-on-Disk Wear Testing Method for Simulating Wear of Polyethylene on Cobalt-Chrome Alloy in Total Hip Arthroplasty."

Turell, M., Friedlaender, G., Wang, A., Thornhill, T., & Bellare, A., (2005) "The effect of counterface roughness onthe wear of UHMWPE for rectangular wear paths".

Escudeiro, A., Wimmer, M., Polcar, T & Cavaleiro, A. (2015) "Tribological behavior of uncoated and DLC- coated CoCr and Ti-alloys in contact with UHMWPE and PEEK counterbodies".

Baykal, D., Siskey, R., Haider, H., Saikko, V., Ahlroos, T., Kurtz, S. (2013) " Advances in tribological testing of artificial joint biomaterials using multidirectional pin-on- disk testers".

Saikko, V., & Kostamo, J. (2011) "RandomPOD – A new method and device for advanced wear simulation of orthopaedic".

ASTM International (2006) ASTM G732-00 "Standard Test Method for wear Testing of Polymeric Materials Used in Total Joint Prostheses"

ASTM International (2002) ASTM G133-95 "Standard Test Method for Linearly Reciprocating Ball-on-Flat Sliding Wear"

ASTM International (2017) ASTM G99-17 "Standard Test Method for Wear Testing with a Pin-on-Disk Apparatus"

ASTM International (2016) ASTM E4 "Standard Practices for Force Verification of Testing Machines"

ASTM International (2018) ASTM E74 "Standard Practices for Calibration and Verification for Force-Measuring Instruments"

Plint Tribology, Web page of commercial tribometers http://www.plint-tribology.com/products/tribometers

CSM – Instruments, Web page of commercial tribometers http:// www.csm-instruments.com/en/High-Temperature-Tribometers

Instrumentacion Nanovea, Web page of commercial tribometers http://www.nanovea.com/tribometers

Auerkari P., (1996) “Mechanical and physical properties of engineering alumina ceramics”, Technical Research Centre of Finland, 26 pp.

Smith, E., (1998) “Mechanical Engineers Reference Book”, 12nd edition, Butterworth Heinemann, 1248 pp.

Linares, O., (2005) “Tribologia y mantenimiento proactivo” American Society of Mechanical Engineers, 10 pp.

Schwenke, T., Wimmer, M., (2013) “Cross-Shear in Metal-on-Polyethylene Articulation of Orthopaedic Implants and its Relationship to Wear".

Saikko, V., (2014) “In vitro wear simulation on the RandomPOD wear testing system as a screening method for bearing materials intended for total knee arthroplasty”.

Kang, L., Galvin, A., Brown, T., Jin, Z., Fisher, J., (2008) “Quantification of the Effect of Cross-shear on the Wear of Conventional and Highly Cross-linked UHMWPE”

Ortega, J., Hernandez, M., Michalczewski, R., (2016) “Micro-Abrasive Wear Testing of Surface Engineered Surgical Grade CoCrMo Alloy for Biotribological Applications”.

Alvarez, M., Ortega, J., Hernandez, M., (2013) “A study of the wear performance in a hip simulator of a metal–metal Co–Cr alloy with different boron additions”.

Thepsatorn, P., Numsomran, A., Tipsuwanporn, V., (2006) “DC Motor Speed Control using Fuzzy Logic based on LabVIEW”

VPG Transducers (2015) “Load Cell Technology” Technical Note VPGT 01, Load cells and weigh modules. www.vpgtransducers.com

LLC, Tacuna Systems (2017) "The Essential Guide to Load Cells: Load Cells, Amplifiers, Calibration, Strain Gauges – Tacuna Systems".

Rangel Carrillo, J. (2007) “Desarrollo de un Sistema de Control para un Simulador de Cadera Mecanico”, Consejo Nacional de Ciencia y Tecnología, Corporación mexicana de Investigación de Materiales.

Isaac, G., Thompson, J., Williams, S., Fisher, J., (2006) “Metal-on-metal bearings surfaces: materials, manufacture, design, optimization and alternatives”.

Turell, M., Wang, A., Bellare, A., (2003) “Quantification of the effect of cross-path motion on the wear rate of ultra high molecular weight polyethylene”.

Korduba, L.A., Wang, A., (2011) – “The effect of cross-shear on the wear of virgin and highly-crosslinked polyethylene”.

APPENDIX

APPENDIX A

STEPPER MOTOR 24HS39-3008D SPECIFICATIONS

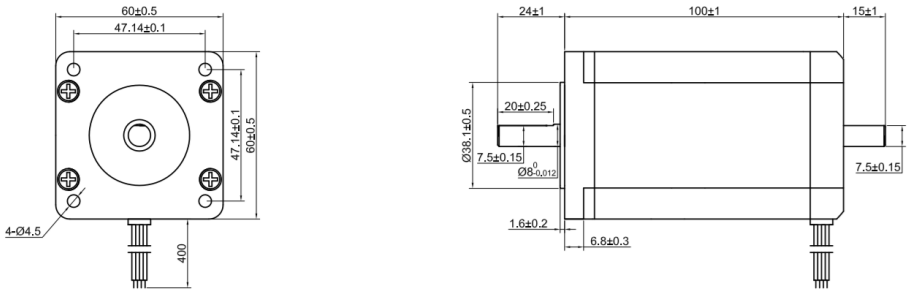

SPECIFICATION \ CONNECTION	UNIPOLAR	BIPOLAR (SERIAL)	BIPOLAR (PARALLEL)
VOTAGE(VOC)	4.20	5.94	2.96
AMPS/PHASE	3.00	2.12	4.24
RESISTANCE/PHASE(Ohms)@25°C	1.40±10%	2.80±10%	0.70±10%
INDUCTANCE/PHASE(mH)@1KHz	3.00±20%	12.00±20%	3.00±20%
HOLDING TORQUE(Nm)[lb-in]	2.80[24.78]	4.00[35.40]	4.00[35.40]
STEP ANGLE(°)	1.80		
STEP ACCURACY(NON-ACCUM)	±5.00%		
ROTOR INERTIA(g-cm²)	980.00		
WEIGHT(Kg)[lb]	1.60[3.53]		
TEMPERATURE RISE:MAX.80°C（MOTOR STANDSTILL;FOR 2PHASE ENERGIZED）			
AMBIENT TEMPERATURE -10°C~50°C[14°F~122°F]			
INSULATION RESISTANCE 100 Mohm（UNDER NORMAL TEMPERATURE AND HUMIDITY）			
INSULATION CLASS B 130°C[266°F]			
DIELECTRIC STRENGTH 500VAC FOR 1MIN.(BETWEEN THE MOTOR COILS AND THE MOTOR CASE)			
AMBIENT HUMIDITY MAX.85%(NO CONDENSATION)			

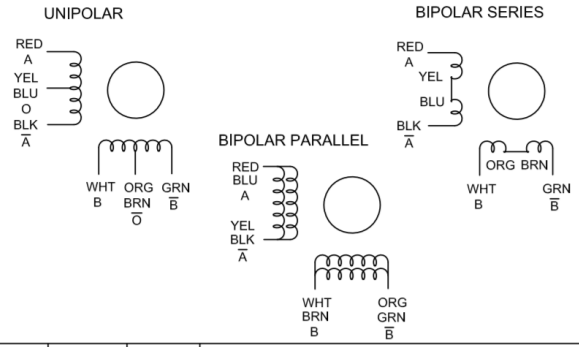

STEPPERONLINE Motors & Electronics

	APVD		STEPPER MOTOR
	CHKD		
1:1.5	DRN		24HS39-3008D
SCALE	SIGNATURE	DATE	

APPENDIX B

MICROSTEP DRIVER M542T SPECIFICATIONS

B.1 Mechanical Specifications

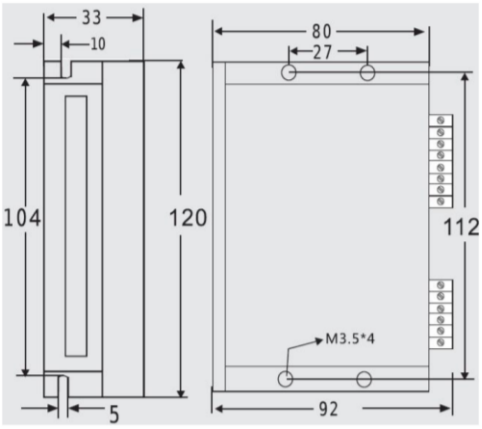

Figure B.1 Mechanical specifications (unit: mm)

B.2 Selecting Microstep Resolution and Driver Output current

This diver used an 8-bit DIP switch to set microstep resolution, and motor current as shown on **Figure B.2.**

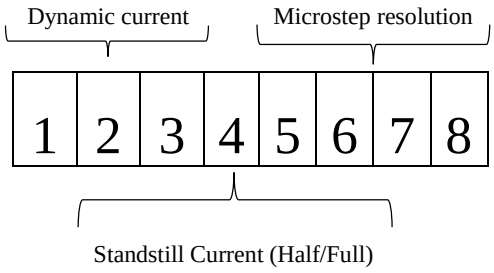

Figure B.2 Distribution of switches on the 8-bit DIP switch

B.2.1 Microstep Resolution Selection

Microstep resolution is set by SW5, 6, 7, 8 of the DIP switch in the following table

Table B.1 Microstep resolution selection

Microstep	Steps/rev.(for 1.8°motor)	SW5	SW6	SW7	SW8
2	400	ON	ON	ON	ON
4	800	ON	OFF	ON	ON
8	1600	ON	ON	OFF	ON
16	3200	ON	OFF	OFF	ON
32	6400	ON	ON	ON	OFF
64	12800	ON	OFF	ON	OFF
128	25600	ON	ON	OFF	OFF
256	51200	ON	OFF	OFF	OFF
5	1000	OFF	ON	ON	ON
10	2000	OFF	OFF	ON	ON
25	5000	OFF	ON	OFF	ON
50	10000	OFF	OFF	OFF	ON
125	25000	OFF	ON	ON	OFF
250	50000	OFF	OFF	ON	OFF

B.2.2 Dynamic current setting

Table B.2 Dynamic current selection

Peak Current	Ref Current (Screen printing)	SW1	SW2	SW3
1.5A	1.0A	ON	ON	ON
2.0A	1.4A	OFF	ON	ON
2.4A	1.7A	ON	OFF	ON
2.8A	2.0A	OFF	OFF	ON
3.2A	2.3A	ON	ON	OFF
3.7A	2.6A	OFF	ON	OFF
4.2A	3.0A	ON	OFF	OFF
4.5A	3.2A	OFF	OFF	OFF

B.3 Sequence Chart of Control Signals

In order to avoid some fault operations and deviations, PUL, DIR and ENA should abide by some rules, shown as following in the diagram.

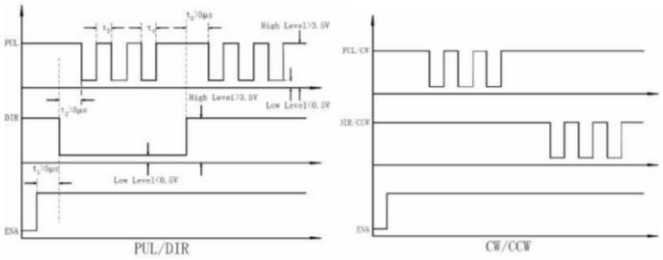

Figure B.3 Sequence chart of control signals

APPENDIX C

LINEAR ACTUATOR SPECIFICATIONS

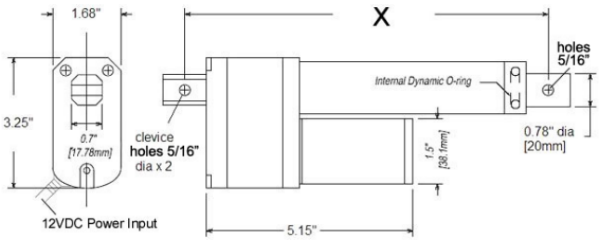

X = Center to Center		
Stroke	**Retracted**	**Extended**
5.90"	11.69"	17.59"

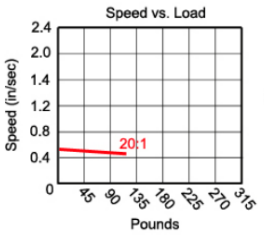

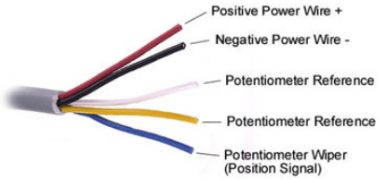

Feedback Wiring Schematic:
White - 10K Pot Reference
Blue - 10K Pot Wiper (Position Signal)
Yellow - 10K Pot Reference

Product Weight	43.3 oz
Voltage Range (Recommended)	6V - 12V
Operating Temperature	-26°C ~ +65°C
Speed (No Load)*	0.50" per second
Speed (Max Load)*	0.39" per second
Dynamic Thrust*	115 lbs
Static Load	500 lbs
Current Drain (No-Load)*	700mA
Current Drain (Max Load)*	3.8A
Current Drain (Stall)*	15A
Motor Type	3 Pole Ferrite
Feedback Style	10KΩ Potentiometer
Potentiometer Tolerance	± 5%
Potentiometer Linearity	± 0.25%
Feedback Density	1.66KΩ / inch
Gear Ratio	20:1
Gear Material	Metal Gear Train, Nylon Pinion
Gearbox Style	Straight Cut Spur
Wire Length	24"
Ingress Protection (IP)	IP54
Duty Cycle	25% (25% on, 75% off)
Housing Material	Zinc Alloy
Lead Screw Type	3mm pitch, single thread

APPENDIX D

DC MOTOR DRIVER VNH5019 SPECIFICATIONS

VNH5019A-E

Automotive fully integrated H-bridge motor driver

Features

Type	$R_{DS(on)}$	I_{out}	V_{ccmax}
VNH5019A-E	18 mΩ typ (per leg)	30 A	41 V

- ECOPACK®: lead free and RoHS compliant
- Automotive Grade: compliance with AEC guidelines
- Output current: 30 A
- 3 V CMOS compatible inputs
- Undervoltage and overvoltage shutdown
- High-side and low-side thermal shutdown
- Cross-conduction protection
- Current limitation
- Very low standby power consumption
- PWM operation up to 20 khz
- Protection against:
  - Loss of ground and loss of V_{CC}
- Current sense output proportional to motor current
- Charge pump output for reverse polarity protection
- Output protected against short to ground and short to V_{CC}

Description

The VHN5019A-E is a full bridge motor driver intended for a wide range of automotive applications. The device incorporates a dual monolithic high-side drivers and two low-side switches. The high-side driver switch is designed using STMicroelectronics' well known and proven proprietary VIPower® M0 technology that allows to efficiently integrate on the same die a true

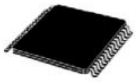

MultiPowerSO-30™

Power MOSFET with an intelligent signal/protection circuit.

The three dice are assembled in MultiPowerSO-30 package on electrically isolated lead-frames. This package, specifically designed for the harsh automotive environment offers improved thermal performance thanks to exposed die pads. The input signals IN_A and IN_B can directly interface to the microcontroller to select the motor direction and the brake condition.

The $DIAG_A/EN_A$ or $DIAG_B/EN_B$, when connected to an external pull-up resistor, enable one leg of the bridge. They also provide a feedback digital diagnostic signal. The CS pin allows to monitor the motor current by delivering a current proportional to its value when CS_DIS pin is driven low or left open. The PWM, up to 20 KHz, lets us to control the speed of the motor in all possible conditions. In all cases, a low-level state on the PWM pin turns-off both the LS_A and LS_B switches. When PWM rises to a high-level, LS_A or LS_B turn-on again depending on the input pin state.

Output current limitation and thermal shutdown protects the concerned high-side in short to ground condition.

The short to battery condition is revealed by the overload detector or by thermal shutdown that latches off the relevant low-side.

Active V_{CC} pin voltage clamp protects the device against low energy spikes in all configurations for the motor.

CP pin provides the necessary gate drive for an external n-channel PowerMOS used for reverse polarity protection.

D.1 Block Diagram and pin description

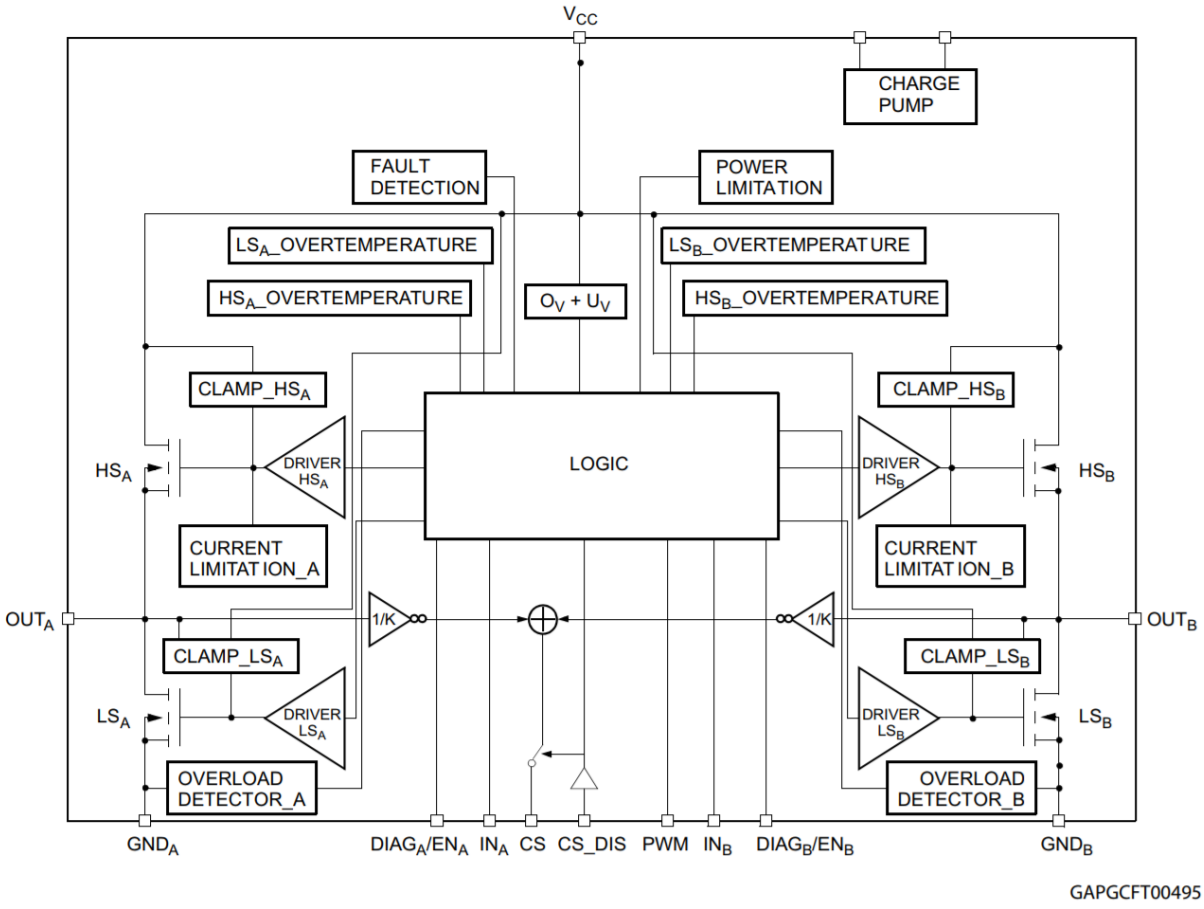

20 KG LOAD CELL (COF) SPECIFICATIONS

APPENDIX E

SMALL LOAD CELL SPECIFICATIONS

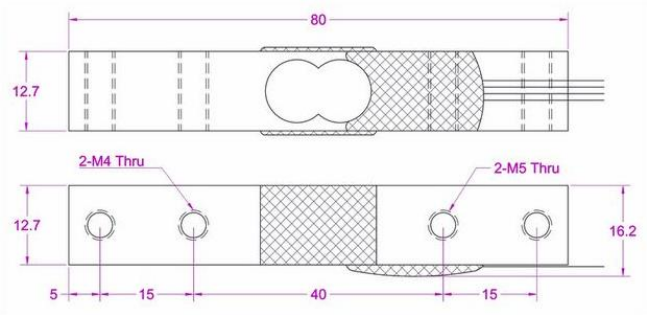

Rated capacity	0.5kg 1kg 2kg 3kg 5kg 6kg 8kg 10kg 15kg 20kg
Rated output	1.0±20%mV/V
Excitation	3-8V
Zero balance	±0.1mV/V.
Non-linearity	±0.05% R.O.
Hysteresis	±0.05% R.O.
Non-repeatability	±0.05% R.O.
Creep(2min)	±0.05% R.O.
Safe overload	150% F.S.
Ultimate overload	200% F.S.
Compensated temperature	0...+25°C
Operating temperature	-10...+40°C
Temperature shift zero	±0.01% R.O./°C
Temperature shift span	±0.05% R.O./10°C
Input resistance	1100±50 ohms
Output resistance	1000±10 ohms
Insulation resistance	>2000M ohms
Ingress protection	IP62
Material of element	Aluminum alloy
Cable	32AWG*120mm(Longer cable available)
Wiring code	Red--Exc+ Black--Exc- Green--Sig+ White--Sig-

APPENDIX F

LOAD CELL YZC-1B SPECIFICATIONS

YZC- 1B series load cell

Features:
Signal point beam load cell, aluminum, colorless anodized, rubber sealed, applied with price computing scale, bench scale etc.

Size:

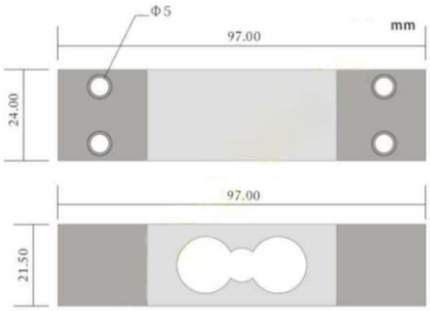

Size: 97x24x22MM
Line:
- **Vcc : Red**
- **GND: Back**
- **Data + : White**
- **Data -: Green**

Full Scale = Vx2.0mA

Technical parameter:

Application	**Price computing scales, bench scale etc.**
Model	**YZC-1B**
Capacity (kg)	**2,3,5,6,8,10,30,35,40,50**
Accuracy class	**C2**
Input resistance Ω	**402±6**
Output resistance Ω	**350±3**
Total error %F.S	≤±0.030
Insulation resistance MΩ	**5000**
Rated output MV/V	**2.0±0.15**
Excitation voltage V	**10~15**
Compensated temperature range	**-10~+40**
Operating temperature range	**-35~+80**
Temperature effect on zero %F.S/	**0.003**
Creep %F.S/30min	**0.03**
Temperature effect on sensitivity %F.S/	**0.0016**
Zero output %F.S	**±1.0**
Safe overload %F.S	**150**
Load cell material	**Aluminum**
Connecting cable	**4.2*350mm**
Method of connecting wire	**Red input(+) back input(-) blue output(+) white output(-)**

Size(in mm,1mm=0.03937inches)

APPENDIX G

G.1 Abbreviations

Al_2O_3 – Aluminum Oxide

CNC – Computer Numerical Control

CoCr – Cobalt Chrome

CVD – Chemical Vapor Deposition

N, KN – Newtons, Kilo Newtons

POD – Pin on Disk

PVD – Physical Vapor Deposition

Ti - Titanium

UHMWPE – Ultra High Molecular Weight Polyethylene

ZrO_2 – Zirconium Dioxide

BIOGRAPHICAL SKETCH

Carlos Aparicio Rodriguez Betancourth graduated on February 2016 with a Bachelor's degree in Mechatronics Engineering, from the Universidad Politecnica de Victoria, in Cd. Victoria, Tamaulipas, México. On September 2015, he started an internship in the University of Texas Rio Grande Valley where he worked with Dr. Jaime Ramos and Dr. Javier Ortega in research. On August 2016 he got accepted into the graduate program of Electrical Engineering and he started working as a Research Assistant under Dr. Javier Ortega in the development of a tribometer for the study of biocompatible materials used in human hip joint implants. He obtained his master's degree on May 2018 at the University of Texas Rio Grande Valley. His email address is carlos.rodriguezbetancourth@gmail.com.